Precise Luminous Flux and Color Control of Dimmable Red-Green-Blue Light-Emitting Diode Systems

Cheuk Ping Germaine Wong, Albert Ting Leung Lee, *Member, IEEE*, Kerui Li, Siew-Chong Tan, *Senior Member*, *IEEE,* S. Y. (Ron) Hui, *Fellow*, *IEEE*

***Abstract*—A generic red, green, blue (RGB) LED system encompasses complex interactions of power, heat, light, and color, which pose a major challenge for achieving precise control over luminance and color-mixing in high-quality lighting applications. In this paper, new nonlinear empirical models of a practical RGB LED system with closed-loop control are formulated. They enable precise prediction of luminous flux and color coordinates by using the three distinct reference voltages as the control variables for independent current regulation across the red, green and blue LED strings. The proposed empirical models are experimentally verified by using a hardware prototype of a DC-DC single-inductor three-output (SITO) LED driver with proportional-integral (PI) compensators and time-interleaving control scheme. The measured values of luminous flux and color coordinates agree closely with the predicted values from the models.**

***Index Terms*—Luminous flux, color coordinates, red-green-blue (RGB) light-emitting diode (LED) system, single-inductor three-output (SITO) LED driver.**

I. INTRODUCTION

Precise illumination and color control in red-green-blue (RGB) light-emitting diode (LED) systems remains a grand challenge facing researchers and engineers in the lighting industry. Typically, a dimmable RGB lamp combines the three primary colors, namely, red, green and blue, in different intensities to produce a broad array of colors. Nowadays, a myriad of RGB intelligent LED solutions such as Philips Hue, Osram Lightfy, Ikea Trådfri or Xiaomi Yeelight have been developed for various color tunable ambient and mood lighting applications. Yet, in practice, the preciseness and performance of dimming and color mixing are still far from satisfactory. This is mainly attributed to the fact that such LED products are based on simplistic linear control methodologies that do not take into account the actual nonlinear characteristic of the LEDs [1]–[12]. Although they can attain the basic functions of dimming and color control, the resulting lighting control is highly inaccurate and inconsistent [1]–[3],[12].

In general, an LED system involves complex interactions of power, heat, light and color. Such interdependence transpires physically that a change in the LED power leads to a corresponding change in the light intensity and junction temperature, which in turn causes an unwanted shift in the color coordinates [12], [13]. Such color deviation can be perceived by the human eye. On the other hand, the existing multicolored LED systems adopt the conventional linear approach, which assumes that the color coordinates of red, green and blue LEDs remain constant. They employ either analog or PWM dimming to perform color mixing. Unfortunately, such an assumption fails to take into consideration the thermal interdependence among the LEDs, which accounts for their inability in achieving precise dimming and color control. To address these issues, a closed-loop nonlinear scheme for precisely controlling the luminous flux and correlated color temperature (CCT) has been introduced for a bicolor white LED system [14], [15]. Nonetheless, it requires the use of a dedicated color sensor to perform optical feedback for attaining precise dimming and CCT control. Also, this approach is only applicable to a simple bicolor white LED lamp comprising warm-white and cool-white LEDs.

Recently, a precise color control scheme based on the empirical nonlinear color model was proposed for RGB LED systems [13]. Compared with the conventional linear approach, the nonlinear approach reported in [13] significantly reduces the color deviation between the measured color point and the target color point. Nonetheless, the RGB LEDs were driven by benchtop power supplies in an open-loop configuration without current regulation. In the absence of any feedback control, the LED current is virtually uncontrollable. The actual LED current value would be different from the desired target value. It should also be noted that the empirical color models were formulated by assuming that the nominal currents across the red, green and blue LEDs are identical. But, in practice, they could be different from each other. Unfortunately, the empirical models do not account for any potential current mismatch across the three LED strings. This implies that the nonlinear color control method in [13] cannot be readily applied to a practical multistring LED system with closed-loop current control. In addition, the theoretical underpinning and empirical model for achieving precise dimming in RGB LED systems are not yet covered.

In view of the aforementioned issues, this paper presents a precise dimming and color control method for a real RGB system with accurate and independent current regulation across the three LED strings. Based on the single-inductor multiple-output (SIMO) power converter architecture [16]–[26], a DC-DC single-inductor three-output (SITO) buck-type LED driver with a reconfigurable digital controller is constructed. Due to

C. P. G. Wong is with the Department of Electrical & Electronic Engineering, The University of Hong Kong (email: gmwong@connect.hku.hk)
A. T. L. Lee is with the Department of Electrical & Electronics Engineering, The University of Hong Kong (email: tlalee@eee.hku.hk)
K. Li is with the Department of Electrical & Electronic Engineering, The University of Hong Kong (email: krli@connect.hku.hk).
S.-C. Tan is with the Department of Electrical & Electronic Engineering, The University of Hong Kong (email: sctan@eee.hku.hk)
S. Y. R. Hui was with the Department of Electrical & Electronic Engineering, The University of Hong Kong and is now with the School of Electrical & Electronic Engineering, Nanyang Technological University, Singapore, (ron.hui@ntu.edu.sg). He is also with the Department of Electrical & Electronic Engineering, Imperial College London (r.hui@imperial.ac.uk).

the use of a single inductor to drive multiple LED strings, the SIMO topology is chosen in order to realize a compact, low-cost and scalable multi-string LED driver. The nominal current in each of the three LED strings can be precisely and independently controlled by adjusting the corresponding reference voltage. Nonlinear empirical luminous flux and color models for precise dimming and color control are formulated by using the three reference voltages as control variables of this tricolor system. The proposed control method can be easily implemented in any RGB LED systems for practical lighting applications. The close agreement between the model predictions and the measured results confirm the validity of the tricolor models and the control scheme. The paper is organized as follows. Section II introduces the concept of brightness and color control of a single-inductor three-output (SITO) LED driver for RGB systems. Section III presents the nonlinear empirical luminous flux and color models. Section IV compares the experimental results of color prediction based on the conventional linear and the proposed nonlinear method. Finally, Section V draws the conclusions of this research work.

II. Brightness and Color Control of SITO LED Driver for RGB Systems

The DC-DC single-inductor three-output (SITO) LED driver transforms a single DC input voltage (V_{in}) into three individual DC output currents (I_R, I_G, I_B), where I_R is the current across the red LED string, I_G is the current across the green LED string, and I_B is the current across the blue LED string. Fig. 1 shows the circuit diagram of a DC-DC buck SITO LED driver with closed-loop control. Since a typical RGB LED system comprises at least three LED strings, three feedback loops, one per LED string, are required for independent current regulation.

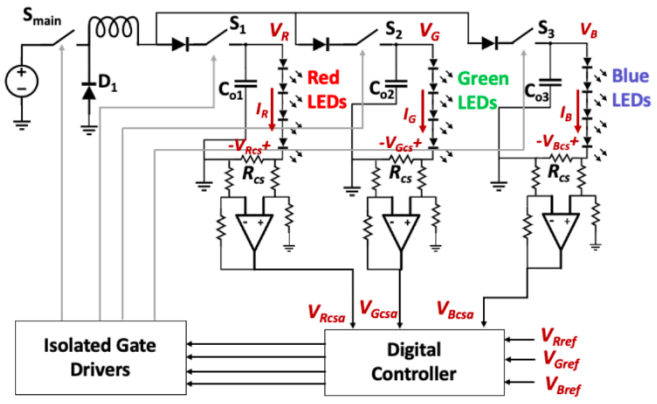

Fig. 1. Circuit diagram of SITO LED driver with feedback control.

A small current sense resistor is connected in series with each LED string. The voltage across each current sense resistor (V_{Rcs}, V_{Gcs}, V_{Bcs}) is amplified by the op amp and then fed into the digital controller. A 32-bit 150 MHz microcontroller (MCU) development board [27] is used to implement the digital controller. An on-board analog-to-digital converter (ADC) transforms the amplified current sense voltages (V_{Rcsa}, V_{Gcsa}, V_{Bcsa}) into their digital counterpart, which are then subtracted from the corresponding reference voltages (V_{Rref}, V_{Gref}, V_{Bref}) in order to generate the error signals. Each error signal is fed into the proportional-integral (PI) compensator in series with the PWM modulator and a limiter to generate a PWM signal with a certain on-time duty ratio (D_R, D_G or D_B) A 3-to-1 multiplexer is used to select one of the three PWM signals to be fed to the input of the isolated gate driver, which generates the gate-drive signal for the main switch ($v_{gs,main}$) of the SITO LED driver. An embedded C program is used to implement the functions of the digital controller shown in Fig. 2.

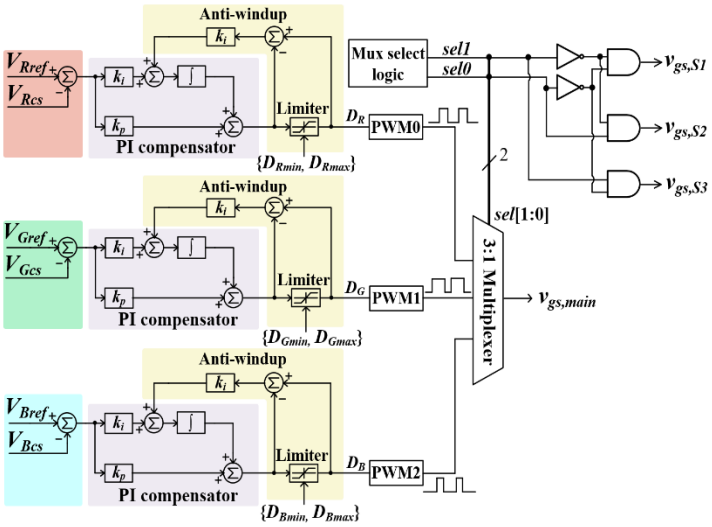

Fig. 2. Functional block diagram of the digital controller.

Proper values of k_p and k_i are chosen for the PI compensator to attain accurate and stable regulation of the current-sense voltage (or LED current). An anti-windup scheme is used to avoid overflow of the integrator and maintain linear operation of the PI compensator. The digital controller ensures that the nominal current in each LED string tracks closely with the corresponding reference voltage. The three reference voltages become the control variables in the closed-loop RGB system. In practice, the current in the three LED strings can be precisely and independently regulated by employing three distinct reference voltages.

Despite the fact that the SITO LED driver with feedback control has been reported in the literature [23], [25], the relationship between the electrical and optical properties of such kind of LED driver is not well understood. Hence, to fill the gap in our understanding, the effect of the variations of the three reference voltages on the luminous flux and color point is formally investigated. The theoretical model of the luminous flux as a function of the three reference voltages will be analytically derived. Subsequently, nonlinear empirical flux and color models will be formulated, which enable us to accurately predict the luminous flux and color point of the RGB LED system for any given set of reference voltages. This eliminates the need to physically measure these parameters in the laboratory using expensive test equipment such as the PMS-50 Spectrophotocolorimeter [28] and an integrating sphere, which is a tedious and time-consuming process.

Let ϕ_T be the total luminous flux of an RGB LED system, ϕ_R be the luminous flux emitted by the red LED only, ϕ_G be the luminous flux emitted by the green LED only, and ϕ_B be the luminous flux emitted by the blue LED only.

$$\phi_T = \phi_R + \phi_G + \phi_B \tag{1}$$

In general, the luminous flux (ϕ) of an LED system can be expressed as

$$\phi = N \times E \times P_{LED} \tag{2}$$

where N is the number of LEDs, E is the luminous efficacy (lumen/Watt) per LED and P_{LED} is the electrical power of a single LED (W).

By combining (1) and (2), we have

$$\phi_T = N_R \times E_R \times P_R + N_G \times E_G \times P_G + N_B \times E_B \times P_B \tag{3}$$

For ease of discussion, suppose $N_R = N_G = N_B = N$ and $E_R = E_G = E_B = E$. Equation (3) can be simplified as follows.

$$\phi_T = N \times E \times \left(P_R + P_G + P_B\right) \tag{4}$$

where P_R, P_G and P_B represent the electrical power of the red, green and blue LED, respectively.

The LED power (P_{LED}) can be defined as $P_{LED} = V_{LED} \times I_{LED}$, where V_{LED} is the LED voltage and I_{LED} is the LED current. Hence, equation (4) can be re-expressed as follows.

$$\phi_T = N \times E \times \left(V_R \times I_R + V_G \times I_G + V_B \times I_B\right) \tag{5}$$

where (V_R, V_G, V_B) represent the voltage across the red, green and blue LED and (I_R, I_G, I_B) represent the current across the red, green and blue LED, respectively. Since closed-loop control is used in the RGB system, as shown in Fig. 1, the DC current (I_R, I_G, I_B) in each of the red, green or blue LED strings is independently regulated by the corresponding reference voltage (V_{Rref}, V_{Gref}, V_{Bref}). Under steady-state condition, the amplified current sense voltage (V_{Rcsa}, V_{Gcsa}, V_{Bcsa}) is the same as the corresponding reference voltage, i.e., $V_{Rcsa} = V_{Rref}$, $V_{Gcsa} = V_{Gref}$, and $V_{Bcsa} = V_{Bref}$. In principle, the LED current can be expressed in terms of the current sense resistor (R_{cs}), the gain of the current sense amplifier (G_{cs}), and the reference voltage. For simplicity, the values of G_{cs} and R_{cs} are assumed to be identical across the three LED strings. However, the current sense voltages can be different due to unbalanced current across the three LED strings. Thus, the current sense voltages are uniquely represented as (V_{Rcs}, V_{Gcs}, V_{Bcs}).

$$\begin{cases} I_R = \dfrac{V_{Rcs}}{R_{cs}} = \dfrac{V_{Rref}}{G_{cs}R_{cs}} = kV_{Rref} \\ I_G = \dfrac{V_{Gcs}}{R_{cs}} = \dfrac{V_{Gref}}{G_{cs}R_{cs}} = kV_{Gref} \\ I_B = \dfrac{V_{Bcs}}{R_{cs}} = \dfrac{V_{Bref}}{G_{cs}R_{cs}} = kV_{Bref} \end{cases} \tag{6}$$

where $k = \dfrac{1}{G_{cs}R_{cs}}$.

Hence, the total luminous flux of an RGB LED system can be formally expressed as

$$\phi_T = N \times E \times k\left(V_R \times V_{Rref} + V_G \times V_{Gref} + V_B \times V_{Bref}\right) \tag{7}$$

In general, the total luminous flux can be expressed as a function of the three distinct reference voltages as follows.

$$\phi_T = k_R V_{Rref} + k_G V_{Gref} + k_B V_{Bref} \tag{8}$$

where k_R, k_G and k_B are parametric constants given in equation (9).

$$\begin{cases} k_R = N \times E \times k \times V_R \\ k_G = N \times E \times k \times V_G \\ k_B = N \times E \times k \times V_B \end{cases} \tag{9}$$

Equation (9) assumes the number of red, green or blue LEDs (N), luminous efficacy (E), the gain of operational amplifier (G_{cs}) and the value of current sense resistor (R_{cs}) are constants.

Equation (8) shows that the total luminous flux is a linear combination of the three reference voltages. Based on this linear relationship, an increase in one of the three reference voltages leads to a proportional increase in the luminous flux. However, this simplistic linear model does not include the thermal aspects of the LED system. In [7], a general photoelectrothermal (PET) theory was developed, which integrates the photometric, electrical, and thermal properties of an LED system. According to the PET theory, the total luminous flux can be modeled as

$$\phi_T = \alpha_1 P_{LED} - \alpha_2 {P_{LED}}^2 \tag{10}$$

where α_1 and α_2 are parametric constants that depend on the rated efficacy (E_o) at room temperature, the heat coefficient (k_h), the electrical coefficient (k_e), the thermal resistance of the heatsink (R_{hs}), and the LED's junction-to-case resistance (R_{jc}) [7]. For an RGB system, equation (10) can be re-expressed as

$$\phi_T = \alpha_1 P_{RGB} - \alpha_2 {P_{RGB}}^2 \tag{11}$$

where P_{RGB} is defined as the "per unit" power of one red LED, one green LED and one blue LED, i.e., $P_{RGB} = P_R + P_B + P_G$.

Similar to (7), P_{RGB} can be expressed in terms of the three reference voltages, i.e.,

$$P_{RGB} = k\left(V_R \times V_{Rref} + V_G \times V_{Gref} + V_B \times V_{Bref}\right) \tag{12}$$

By substituting (12) into (11) and re-arranging, we have

$$\begin{aligned} \phi_T = {} & -\alpha_2 k^2 {V_R}^2 {V_{Rref}}^2 + \alpha_1 k V_R V_{Rref} - 2\alpha_2 k^2 V_R V_G V_{Rref} V_{Gref} \\ & -\alpha_2 k^2 {V_G}^2 {V_{Gref}}^2 + \alpha_1 k V_G V_{Gref} - 2\alpha_2 k^2 V_G V_B V_{Gref} V_{Bref} \\ & -\alpha_2 k^2 {V_B}^2 {V_{Bref}}^2 + \alpha_1 k V_B V_{Bref} - 2\alpha_2 k^2 V_B V_R V_{Bref} V_{Rref} \end{aligned} \tag{13}$$

Equation (13) defines the general nonlinear model of the luminous flux as a function of the three reference voltages (V_{Rref}, V_{Gref}, V_{Bref}). It is a second degree polynomial. For a given set of reference voltages (V_{Rref}, V_{Gref}, V_{Bref}), the corresponding current values (I_R, I_G, I_B) can be determined from (6). By referring to the I-V curve of the red, green or blue LED from the datasheet, the corresponding values of (V_R, V_G, V_B) can also be obtained. The total luminous flux ϕ_T can therefore be calculated from (13). It is interesting to note that if α_2 is zero, equation (13) reduces to (8), which means that the linear flux model is a special case of the nonlinear flux model.

In general, the number of red, green and blue LEDs may *not* be the same in the RGB LED system. Suppose the system contains distinct numbers of red, green and blue LEDs, where N_R, N_G and

N_B are the number of red, green and blue LEDs, respectively. The power of one red LED, one green LED and one blue LED can be expressed as

$$\begin{cases} P_R = V_R I_R = kV_R V_{Rref} \\ P_G = V_G I_G = kV_G V_{Gref} \\ P_B = V_B I_B = kV_B V_{Bref} \end{cases} \tag{14}$$

Equation (10) can therefore be re-expressed in terms P_R, P_G and P_B as follows.

$$\phi_T = \alpha_1 (N_R P_R + N_G P_G + N_B P_B) - \alpha_2 (N_R P_R + N_G P_G + N_B P_B)^2 \tag{15}$$

By substituting (14) into (15) and re-arranging, we have

$$\begin{aligned} \phi_T = & -\alpha_2 k^2 k_R{}^2 V_{Rref}{}^2 + \alpha_1 k k_R V_{Rref} - 2\alpha_2 k^2 k_R k_G V_{Rref} V_{Gref} \\ & -\alpha_2 k^2 k_G{}^2 V_{Gref}{}^2 + \alpha_1 k k_G V_{Gref} - 2\alpha_2 k^2 k_G k_B V_{Gref} V_{Bref} \\ & -\alpha_2 k^2 k_B{}^2 V_{Bref}{}^2 + \alpha_1 k k_B V_{Bref} - 2\alpha_2 k^2 k_B k_R V_{Bref} V_{Rref} \end{aligned} \tag{16}$$

It is interesting to note that equation (16) resembles equation (13), both of which are second degree polynomial. Equation (16) represents a more generalized nonlinear flux model because the number of red, green and blue LEDs can be the same or different.

In the study of color science, one of the first mathematically defined color spaces is the CIE 1931 color system created by the International Commission on Illumination (CIE) in 1931. For a given power-spectral density $P(\lambda)$, the XYZ tristimulus values are defined as follows [29].

$$X = \int_{\lambda} \bar{x}(\lambda) P(\lambda) d\lambda \tag{17a}$$

$$Y = \int_{\lambda} \bar{y}(\lambda) P(\lambda) d\lambda \tag{17b}$$

$$Z = \int_{\lambda} \bar{z}(\lambda) P(\lambda) d\lambda \tag{17c}$$

where $\bar{x}(\lambda), \bar{y}(\lambda)$ and $\bar{z}(\lambda)$ are the color-matching functions, which are the numerical description of the chromatic response of the CIE standard observer. In practice, the CIE xyY color space is often used to specify colors. Basically, the chromaticity of a certain color is specified by the (x, y) color coordinates. Fig. 3 shows the CIE 1931 color space chromaticity diagram.

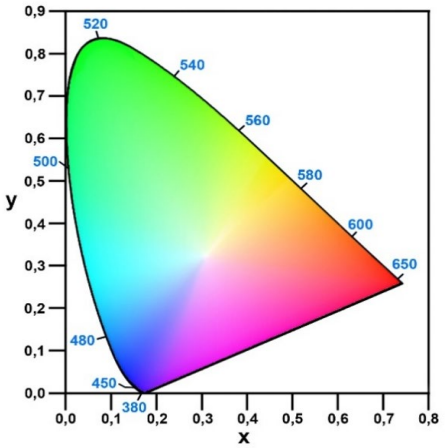

Fig. 3. CIE 1931 color space chromaticity diagram.

The Y parameter is a quantitative measure of the brightness (or luminance) of a color. The values of (x, y) can be obtained from the normalization of the XYZ tristimulus values, that is,

$$\begin{cases} x = \dfrac{X}{X+Y+Z} \\ y = \dfrac{Y}{X+Y+Z} \end{cases} \tag{18}$$

The CIE 1931 color space is superceded by the CIE 1960 Uniform Color Space (UCS) with uniform (u, v) color coordinates. The (u, v) color coordinates can be obtained from the XYZ tristimulus values as follows.

$$\begin{cases} u = \dfrac{4X}{X+15Y+3Z} \\ v = \dfrac{6Y}{X+15Y+3Z} \end{cases} \tag{19}$$

For the sake of quantifying the color deviation of a light source, a new parameter Δuv is defined as

$$\Delta uv = \sqrt{(u-u_o)^2 + (v-v_o)^2} \tag{20}$$

where (u, v) is the actual color coordinates of the light source and (u_o, v_o) is the target color coordinates. Δuv is the Euclidean distance between the actual color point and the target color point, which represents the deviation of the actual color point from the target one. The specifications of color tolerance for LED sources are given in [30].

Color mixing in the existing RGB LED lamps are primarily based on simple linear color averaging of the red, green and blue LEDs. A certain color can be produced by a linear combination of the three primary colors, which is the fundamental concept of colorimetry [31], [32]. In other words, the total tristimulus value (X_T, Y_T, Z_T) is a linear combination of (X_R, Y_R, Z_R) units of red color, (X_G, Y_G, Z_G) units of green color, and (X_B, Y_B, Z_B) units of blue color. Mathematically, it can be written as

$$\begin{bmatrix} X_T(V_{Rref}, V_{Gref}, V_{Bref}) \\ Y_T(V_{Rref}, V_{Gref}, V_{Bref}) \\ Z_T(V_{Rref}, V_{Gref}, V_{Bref}) \end{bmatrix} = \begin{bmatrix} X_R(V_{Rref}) \\ Y_R(V_{Rref}) \\ Z_R(V_{Rref}) \end{bmatrix} + \begin{bmatrix} X_G(V_{Gref}) \\ Y_G(V_{Gref}) \\ Z_G(V_{Gref}) \end{bmatrix} + \begin{bmatrix} X_B(V_{Bref}) \\ Y_B(V_{Bref}) \\ Z_B(V_{Bref}) \end{bmatrix} \tag{21}$$

where V_{Rref}, V_{Gref} and V_{Bref} are the reference voltages, and X_R, X_G and X_B are the tristimulus values of the red, green and blue LEDs, respectively. (X_T, Y_T, Z_T) are the total tristimulus values of the resulting color mixture. A major limitation of the simplistic linear approach is that it neglects the non-ideal factors such as the effect of temperature variation on tristimulus values and the thermal interdependency among the three different types of LEDs [13], [31], [32]. The inaccuracy of the linear model in predicting the color point has already been proven in [13]. Hence, in the following section, a new nonlinear empirical color model for a closed-loop RGB system will be discussed in detail.

III. New Nonlinear Luminance and Color Model for Closed-Loop RGB Systems

According to the PET theory [7], a portion of the LED power is dissipated as heat. The color of the LED depends on the junction temperature, which is a function of the LED power, current driving technique, heatsink material and size as well as the ambient temperature (T_a). Fig. 4 shows a simplified thermal

model of an RGB LED system. The junction-to-case thermal resistance of the red, green and blue LED are modeled by $R_{R,jc}$, $R_{G,jc}$ and $R_{B,jc}$, respectively. Since the three LEDs are mounted on the same heatsink, $R_{R,hs}$, $R_{G,hs}$, $R_{B,hs}$ are the thermal resistance between the corresponding LED and the heatsink. In addition, each LED is subject to the heat dissipated by its neighboring LEDs. For example, the red LED will be thermally coupled to the green and blue LEDs. Hence, R_{RG}, R_{RB} and R_{GB} represent the thermal resistance between two adjacent LEDs, as depicted in Fig. 4. The actual arrangement of the LEDs will affect the values of the thermal resistance. In the proposed nonlinear empirical luminous flux and color models for closed-loop RGB systems, such thermal interdependency will be taken into consideration.

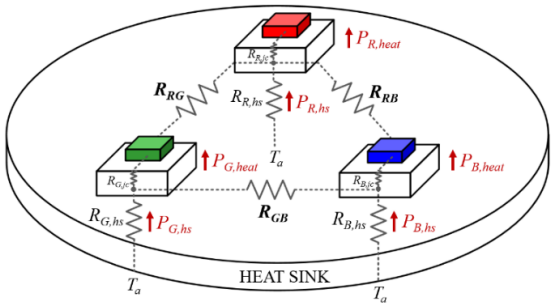

Fig. 4. A simple thermal model of an RGB LED system.

A. Nonlinear Empirical Luminous Flux Model

Based on the SITO LED driver with feedback control shown in Fig. 1, the nonlinear empirical luminous flux model is obtained by varying the three reference voltages (V_{Rref}, V_{Gref}, V_{Bref}) accordingly and measuring the total luminous flux. The following procedures are performed during the measurement. Fig. A1 in the Appendix contains a flowchart which provides a graphical illustration of these procedures.

1. Mount the red, green and blue LEDs on the same heatsink which are placed inside the integrating sphere.
2. Connect the first, second and third output of the SITO LED driver with feedback control to the red, green and blue LED string, respectively.
3. The current value of the red LED (I_R) is varied incrementally from 50 mA to 550 mA with a step size of 50 mA while the current values of the green LED and blue LEDs (I_G, I_B) are kept constant. By applying closed-loop control, the value of I_R can be varied by adjusting the corresponding normalized reference voltage (V_{Rref}) from 0.1 V to 1.0 V with a step size of 80 mV. The general relationship between I_R and V_{Rref} is given by (6). For each sweep of V_{Rref} values, the reference voltage values of the green and blue LEDs (V_{Gref}, V_{Bref}) are kept constant (e.g. V_{Gref} = 0.5 V and V_{Bref} = 0.5 V). Intuitively, as the value of V_{Rref} increases, a larger current will flow across the red LEDs which leads to an increase in the total luminous flux of the emitted light. Because the values of V_{Gref} and V_{Bref} are fixed, the heat dissipated by the green and blue LEDs in steady-state condition is constant. As a result, the luminous flux is measured at the two boundary conditions: 1. Minimum thermal energy of the green and blue LEDs will be produced when they are maximally dimmed (by setting V_{Gref} = 0.1 and V_{Bref} = 0.1 V); 2. Maximum thermal energy of the green and blue LEDs will be generated when they are fully turned ON (by setting V_{Gref} = 1 V and V_{Bref} = 1 V). In addition, a third (middle) case is considered (i.e., V_{Gref} = 0.5 V and V_{Bref} = 0.5 V). Fig. 5 shows the variation of the measured flux (ϕ_m) against V_{Rref} for three distinct sets of (V_{Gref}, V_{Bref}) values. It shows a nonlinear relationship between ϕ_m and V_{Rref}. As V_{Rref} increases, the rate of increase of ϕ_m is reduced. It is also interesting to note that with larger values of (V_{Gref}, V_{Bref}), the luminous flux becomes smaller at a particular value of V_{Rref}. This is attributed to the fact that a larger value of V_{Gref} (or V_{Bref}) means a larger current value of I_G (or I_B), which implies more heat produced by the green (or blue) LED is being transferred to the red LED. Consequently, the red LED becomes dimmer even with the same value of V_{Rref} (or I_R).
4. The current value of the green LED (I_G) is varied in 50 mA increments over a full range of 50 mA to 550 mA while the current values of the red LED and blue LEDs (I_R, I_B) are held constant. I_G can be precisely controlled by adjusting the value of V_{Gref} in 80 mV increments from 0.1 V to 1.0 V while the values of V_{Rref} and V_{Bref} remain unchanged. Fig. 6 shows the variation of ϕ_m versus V_{Gref} for three distinct sets of (V_{Rref}, V_{Bref}) values.
5. The current value of the blue LED (I_B) is changed in 50 mA increments over a full range of 50 mA to 550 mA while the current values of the red LED and green LEDs (I_R, I_G) stay constant. I_B can be precisely controlled by varying V_{Bref} in 80 mV increments from 0.1 V to 1.0 V whereas V_{Rref} and V_{Bref} are held constant. Fig. 7 shows the variation of ϕ_m versus V_{Bref} for three different sets of (V_{Rref}, V_{Gref}) values.

The measurement results contain a total of 104 measured data of (ϕ_m, V_{Rref}, V_{Gref}, V_{Bref}). Fig. 8 shows the measured flux values, which are interpolated by the solid blue curve. Because the theoretical luminous flux equation in (13) has a degree of two, a second degree polynomial is used to best fit the measured data, as shown by the dotted orange curve in Fig. 8. By invoking linear regression with the fitlm function in Matlab, a second-order polynomial function of luminous flux is obtained in (18). Table I contains the values of the nine coefficients in (18).

$$\begin{aligned}\phi_T\left(V_{Rref},V_{Gref},V_{Bref}\right) = {} & \alpha_{R1}V_{Rref}^{\,2}+\alpha_{R2}V_{Rref}+\alpha_{R3}V_{Rref}V_{Gref} \\ & +\beta_{G1}V_{Gref}^{\,2}+\beta_{G2}V_{Gref}+\beta_{G3}V_{Gref}V_{Bref} \\ & +\gamma_{B1}V_{Bref}^{\,2}+\gamma_{B2}V_{Bref}+\gamma_{B3}V_{Bref}V_{Rref} \end{aligned} \quad (22)$$

where α_{R1}-α_{R3}, β_{G1}-β_{G3}, and γ_{B1}-γ_{B3} are the coefficients.

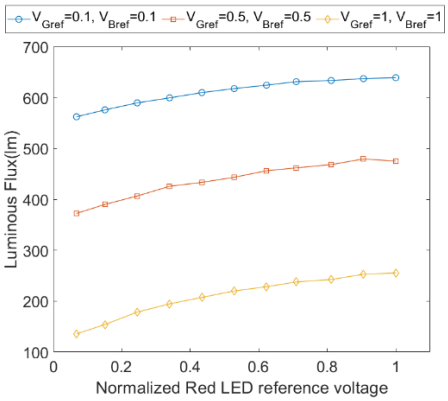

Fig. 5. Measured flux (ϕ_m) versus normalized reference voltage of red LED (V_{Rref}).

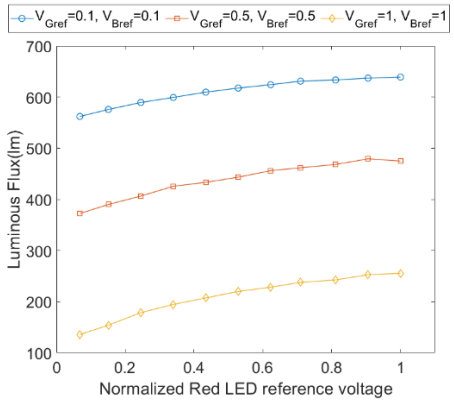

Fig. 6. Measured flux (ϕ_m) versus normalized reference voltage of green LED (V_{Gref}).

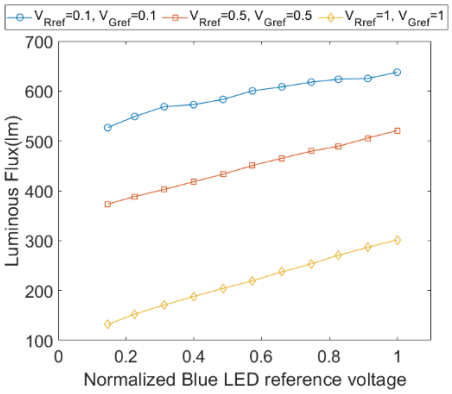

Fig. 7. Measured flux (ϕ_m) versus normalized reference voltage of blue LED (V_{Bref}).

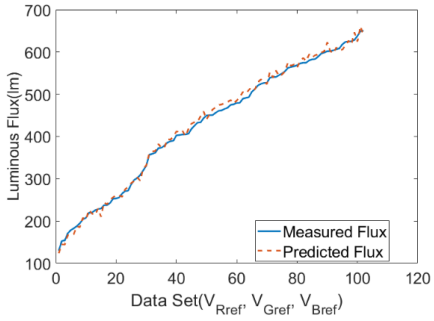

Fig. 8. Measured flux vs. predicted flux from curve fitting function.

TABLE I. VALUES OF THE NINE COEFFICIENTS IN (18).

α_{R1}	α_{R2}	α_{R3}
–117.7415	288.1818	–60.154
β_{G1}	β_{G2}	β_{G3}
–245.2950	652.2079	–32.4688
γ_{B1}	γ_{B2}	γ_{B3}
–72.0415	300.4316	–48.9859

From (22), the total luminous flux can be predicted for any given set of (V_{Rref}, V_{Gref}, V_{Bref}). The mean percentage error between the predicted flux values and the measured ones is only 1.86%. Equation (22) represents the nonlinear empirical model of luminous flux for the closed-loop RGB system. It is worth noting that (22) has the same form as (13), which means that the empirical and theoretical models agree closely with each other. Consider the special case when all LEDs are fully turned OFF (i.e., $V_{Rref} = 0$, $V_{Gref} = 0$, $V_{Bref} = 0$). The empirical model predicts that the luminous flux is zero, i.e., $\phi_T(0, 0, 0) = 0$, which is the expected value. Conversely, when all LEDs are fully turned ON (i.e., $V_{Rref} = 1$, $V_{Gref} = 1$, $V_{Bref} = 1$), the luminous flux attains its maximum value ($\phi_{T,max}$). So, equation (22) can be re-expressed as (23), which is basically the *sum* of all coefficients, that is,

$$\phi_{T,max} = \phi_T(1,1,1) = \sum_{i=1}^{9} \alpha_i \tag{23}$$

By substituting the coefficient values in Table I into (23), $\phi_{T,max}$ is calculated to be around 669.97 lm, which is in good agreement with the measured value of 658.02 lm.

B. Nonlinear Empirical Color Model

In the RGB LED system, the color of each LED chip depends not only on its own junction temperature but also on the heat generated by the neighboring LEDs (assuming that they share the same heatsink) and the ambient temperature. From (18), the (x, y) color coordinates is a function of the (X, Y, Z) tristimulus values. Any variations in the tristimulus values will cause a shift in the color coordinates, thus resulting in a color change of the LED. The thermal coupling among the RGB LEDs will also be taken into consideration in the nonlinear empirical color model. In this investigation, the RGB LEDs are mounted on the same heatsink and connected to the SITO LED driver, the following procedures are performed to construct the nonlinear color model. Fig. A2 in the Appendix contains a flowchart which provides a graphical illustration of these procedures.

1. Treat the red LED as the major color source. The reference voltages of the green and blue LED are set to zero (i.e., $V_{Gref} = 0$ V, $V_{Bref} = 0$ V), which means they are fully switched OFF. This serves as the upper boundary condition in which no heat energy is transmitted from the green and blue LED sources to the red LED source. Perform a sweep of the reference voltage of red LED (V_{Rref}) ranging from 0.1 V to 1 V and measure the tristimulus values of the red LED source (X_R, Y_R, Z_R). Conversely, the reference voltages of the green and blue LED are set to one (i.e., $V_{Gref} = 1$ V, $V_{Bref} = 1$ V) so that they can be fully turned ON. This serves as the lower boundary condition in which maximum heat energy is transmitted from the green and blue LED sources to the red LED source. Then, sweep V_{Rref} from 0.1 V to 1 V and measure the tristimulus values. The same measurement process is replicated for two intermediate cases, namely, green LED is ON and blue LED is OFF ($V_{Gref} = 1$ V, $V_{Bref} = 0$ V), and green LED is OFF and blue LED is ON ($V_{Gref} = 0$ V, $V_{Bref} = 1$ V). It is envisaged that the tristimulus values of these two middle cases should be located within the two boundary conditions. Fig. 9 depicts the measured tristimulus values (X_R, Y_R, Z_R) of the red LED under the four different conditions. It is observed that at a particular V_{Rref} value, maximum tristimulus values of the red LED occur when the green and blue LEDs are OFF. It is because there is no heat energy is transferred from the green and blue LEDs to the red LED. Likewise, minimum tristimulus values of the red LED occur when the green and blue LEDs are fully turned ON. This is attributed to maximum heat transfer from the green and blue LEDs. It becomes apparent that for a given

value of V_{Rref}, the tristimulus values of red LED source under other operating conditions of green and blue LEDs are located somewhere between the maximum and minimum curves. The tristimulus profiles of the red LED in Fig. 9 consistently show that the (X_R, Y_R, Z_R) values are at their maximum value when V_{Rref} is about 0.5 V to 0.6 V, regardless of the operating conditions of the other LEDs. This can be elucidated by the fact that as V_{Rref} continues to rise, a larger current across the red LED further increases the heat dissipation and accumulation within the LED device, thereby leading to the degradation and shift in its color spectrum. Consequently, from (13a)–(13c), the (X_R, Y_R, Z_R) values will decrease at larger values of V_{Rref}.

2. Treat the green LED as the main color source. Both the red and blue LEDs are switched OFF by setting V_{Rref} and V_{Bref} to zero. Sweep V_{Gref} from 0.1 V to 1 V and measure the tristimulus values of the green LED source (X_G, Y_G, Z_G). On the other hand, both the red and blue LEDs are fully switched ON by setting V_{Rref} and V_{Bref} to one. Sweep V_{Gref} from 0.1 V to 1 V and measure the tristimulus values. The same procedure is then repeated for two intermediate cases, i.e., red LED is ON and blue LED is OFF (V_{Rref} = 1, V_{Bref} = 0), and red LED is OFF and blue LED is ON (V_{Rref} = 0, V_{Bref} = 1). Fig. 10 shows the measured (X_G, Y_G, Z_G) values of the green LED under the four operating conditions.
3. Treat the blue LED as the main color source. Both the red and green LEDs are switched OFF by setting V_{Rref} and V_{Gref} to zero. Sweep V_{Bref} incrementally from 0.1 V to 1 V and record the tristimulus values of the blue LED source (X_B, Y_B, Z_B). Contrarily, both the red and green LEDs are fully turned ON by setting V_{Rref} and V_{Gref} to one. Then, sweep V_{Bref} from 0.1 V to 1 V and measure the tristimulus values of the blue LED source. The same steps are repeated for two middle cases, i.e., red LED is ON and green LED is OFF (V_{Rref} = 1, V_{Gref} = 0) and red LED is OFF and green LED is ON (V_{Rref} = 0, V_{Gref} = 1). Fig. 11 shows the measured (X_B, Y_B, Z_B) values of the blue LED for the four operating conditions.

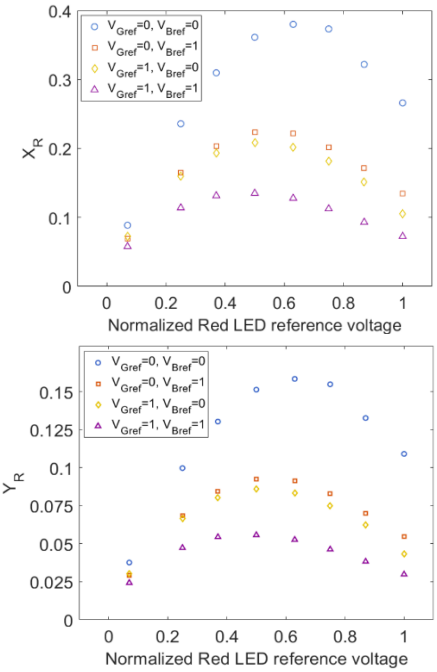

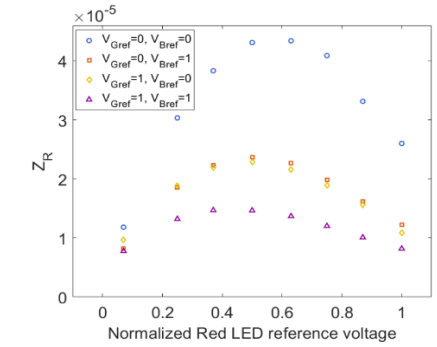

Fig. 9. Measured tristimulus values (X_R, Y_R, Z_R) of the red LED.

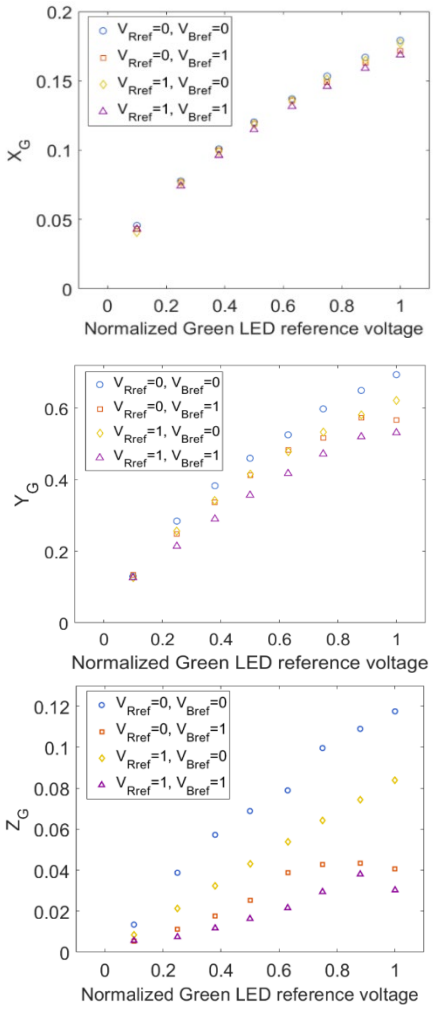

Fig. 10. Measured tristimulus values (X_G, Y_G, Z_G) of the green LED.

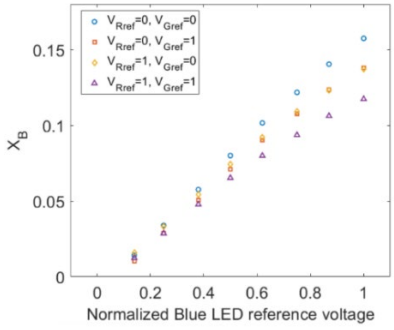

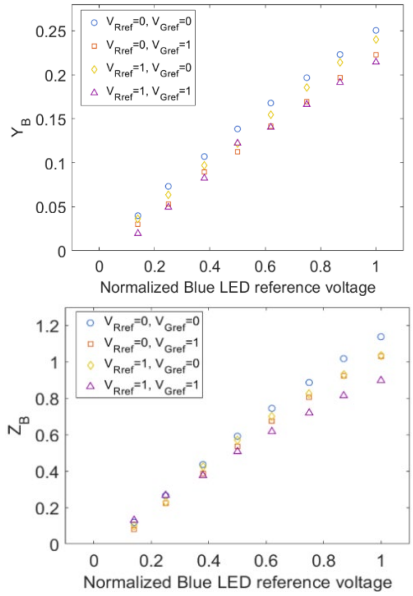

Fig. 11. Measured tristimulus values (X_B, Y_B, Z_B) of the blue LED.

To obtain a best fitting curve for the measured values of (X_R, Y_R, Z_R) of the red LED source in Fig. 9, a third-order polynomial function of the following form is used.

$$\begin{bmatrix} X_R\left(V_{Rref},V_{Gref},V_{Bref}\right) \\ Y_R\left(V_{Rref},V_{Gref},V_{Bref}\right) \\ Z_R\left(V_{Rref},V_{Gref},V_{Bref}\right) \end{bmatrix} = \begin{bmatrix} \alpha_{XR1}\left(V_{Gref},V_{Bref}\right) \\ \alpha_{YR1}\left(V_{Gref},V_{Bref}\right) \\ \alpha_{ZR1}\left(V_{Gref},V_{Bref}\right) \end{bmatrix} V_{Rref}{}^3 + \begin{bmatrix} \beta_{XR1}\left(V_{Gref},V_{Bref}\right) \\ \beta_{YR1}\left(V_{Gref},V_{Bref}\right) \\ \beta_{ZR1}\left(V_{Gref},V_{Bref}\right) \end{bmatrix} V_{Rref}{}^2 + \begin{bmatrix} \gamma_{XR1}\left(V_{Gref},V_{Bref}\right) \\ \gamma_{YR1}\left(V_{Gref},V_{Bref}\right) \\ \gamma_{ZR1}\left(V_{Gref},V_{Bref}\right) \end{bmatrix} V_{Rref}$$

for $0 \le V_{Rref} \le 0.5$. (24a)

$$\begin{bmatrix} X_R\left(V_{Rref},V_{Gref},V_{Bref}\right) \\ Y_R\left(V_{Rref},V_{Gref},V_{Bref}\right) \\ Z_R\left(V_{Rref},V_{Gref},V_{Bref}\right) \end{bmatrix} = \begin{bmatrix} \alpha_{XR2}\left(V_{Gref},V_{Bref}\right) \\ \alpha_{YR2}\left(V_{Gref},V_{Bref}\right) \\ \alpha_{ZR2}\left(V_{Gref},V_{Bref}\right) \end{bmatrix} V_{Rref}{}^3 + \begin{bmatrix} \beta_{XR2}\left(V_{Gref},V_{Bref}\right) \\ \beta_{YR2}\left(V_{Gref},V_{Bref}\right) \\ \beta_{ZR2}\left(V_{Gref},V_{Bref}\right) \end{bmatrix} V_{Rref}{}^2 + \begin{bmatrix} \gamma_{XR2}\left(V_{Gref},V_{Bref}\right) \\ \gamma_{YR2}\left(V_{Gref},V_{Bref}\right) \\ \gamma_{ZR2}\left(V_{Gref},V_{Bref}\right) \end{bmatrix} V_{Rref}$$

for $0.5 < V_{Rref} \le 1$. (24b)

where α_{XR1}, β_{XR1}, γ_{XR1}, α_{YR1}, β_{YR1}, γ_{YR1}, α_{ZR1}, β_{ZR1}, γ_{ZR1}, α_{XR2}, β_{XR2}, γ_{XR2}, α_{YR2}, β_{YR2}, γ_{YR2}, α_{ZR2}, β_{ZR2} and γ_{ZR2} are functions of two variables (V_{Gref}, V_{Bref}) that model the thermal coupling from the green and blue LED sources to the red one. Equation (24a) and (24b) model the rising and falling sections of the tristimulus curve, respectively. For the tristimulus value of X_R, α_{XR1}, β_{XR1}, γ_{XR1} (or α_{XR2}, β_{XR2}, γ_{XR2}) determine the gradient (slope) of the X_R curve at a particular value of V_{Rref}. The two boundary conditions, i.e., $0 \le V_{Gref} \le 1$ and $0 \le V_{Bref} \le 1$, will produce a range of gradient values. For the tristimulus value of X_R, we have

$$\begin{aligned} &\alpha_{XRG,min1}\left(\alpha_{XRG,min2}\right) \le \alpha_{XR1}\left(\alpha_{XR2}\right) \le \alpha_{XRG,max1}\left(\alpha_{XRG,max2}\right) \\ &\beta_{XRG,min1}\left(\beta_{XRG,min2}\right) \le \beta_{XR1}\left(\beta_{XR2}\right) \le \beta_{XRG,max1}\left(\beta_{XRG,max2}\right) \\ &\gamma_{XRG,min1}\left(\gamma_{XRG,min2}\right) \le \gamma_{XR1}\left(\gamma_{XR2}\right) \le \gamma_{XRG,max1}\left(\gamma_{XRG,max2}\right) \end{aligned} \quad (25)$$

Likewise, for the tristimulus values of Y_R and Z_R, we have

$$\begin{aligned} &\alpha_{YRG,min1}\left(\alpha_{YRG,min2}\right) \le \alpha_{YR1}\left(\alpha_{YR2}\right) \le \alpha_{YRG,max1}\left(\alpha_{YRG,max2}\right) \\ &\beta_{YRG,min1}\left(\beta_{YRG,min2}\right) \le \beta_{YR1}\left(\beta_{YR2}\right) \le \beta_{YRG,max1}\left(\beta_{YRG,max2}\right) \\ &\gamma_{YRG,min1}\left(\gamma_{YRG,min2}\right) \le \gamma_{YR1}\left(\gamma_{YR2}\right) \le \gamma_{YRG,max1}\left(\gamma_{YRG,max2}\right) \end{aligned} \quad (26)$$

$$\begin{aligned} &\alpha_{ZRG,min1}\left(\alpha_{ZRG,min2}\right) \le \alpha_{ZR1}\left(\alpha_{ZR2}\right) \le \alpha_{ZRG,max1}\left(\alpha_{ZRG,max2}\right) \\ &\beta_{ZRG,min1}\left(\beta_{ZRG,min2}\right) \le \beta_{ZR1}\left(\beta_{ZR2}\right) \le \beta_{ZRG,max1}\left(\beta_{ZRG,max2}\right) \\ &\gamma_{ZRG,min1}\left(\gamma_{ZRG,min2}\right) \le \gamma_{ZR1}\left(\gamma_{ZR2}\right) \le \gamma_{ZRG,max1}\left(\gamma_{ZRG,max2}\right) \end{aligned} \quad (27)$$

By applying linear interpolation in the operating region bounded by the respective maximum and minimum values, the functions of α_{XR1}, α_{YR1}, α_{ZR1}, α_{XR2}, α_{YR2} and α_{ZR2} can be expressed as

$$\begin{bmatrix} \alpha_{XR1}\left(V_{Gref},V_{Bref}\right) \\ \alpha_{YR1}\left(V_{Gref},V_{Bref}\right) \\ \alpha_{ZR1}\left(V_{Gref},V_{Bref}\right) \end{bmatrix} = \begin{bmatrix} \alpha_{XR,01} \\ \alpha_{YR,01} \\ \alpha_{ZR,01} \end{bmatrix} + \begin{bmatrix} \alpha_{XRG,max1}-\alpha_{XRG,min1} \\ \alpha_{YRG,max1}-\alpha_{YRG,min1} \\ \alpha_{ZRG,max1}-\gamma_{ZRG,min1} \end{bmatrix} V_{Gref} + \begin{bmatrix} \alpha_{XRB,max1}-\alpha_{XRB,min1} \\ \alpha_{YRB,max1}-\alpha_{YRB,min1} \\ \alpha_{ZRB,max1}-\alpha_{ZRB,min1} \end{bmatrix} V_{Bref} \quad \text{for } 0 \le V_{Rref} \le 0.5 \quad (28a)$$

$$\begin{bmatrix} \alpha_{XR2}\left(V_{Gref},V_{Bref}\right) \\ \alpha_{YR2}\left(V_{Gref},V_{Bref}\right) \\ \alpha_{ZR2}\left(V_{Gref},V_{Bref}\right) \end{bmatrix} = \begin{bmatrix} \alpha_{XR,02} \\ \alpha_{YR,02} \\ \alpha_{ZR,02} \end{bmatrix} + \begin{bmatrix} \alpha_{XRG,max2}-\alpha_{XRG,min2} \\ \alpha_{YRG,max2}-\alpha_{YRG,min2} \\ \alpha_{ZRG,max2}-\gamma_{ZRG,min2} \end{bmatrix} V_{Gref} + \begin{bmatrix} \alpha_{XRB,max2}-\alpha_{XRB,min2} \\ \alpha_{YRB,max2}-\alpha_{YRB,min2} \\ \alpha_{ZRB,max2}-\alpha_{ZRB,min2} \end{bmatrix} V_{Bref} \quad \text{for } 0.5 < V_{Rref} \le 1 \quad (28b)$$

The functions of β_{XR1}, β_{YR1}, β_{ZR1}, β_{XR2}, β_{YR2} and β_{ZR2} can be written in a similar fashion as

$$\begin{bmatrix} \beta_{XR1}\left(V_{Gref},V_{Bref}\right) \\ \beta_{YR1}\left(V_{Gref},V_{Bref}\right) \\ \beta_{ZR1}\left(V_{Gref},V_{Bref}\right) \end{bmatrix} = \begin{bmatrix} \beta_{XR,01} \\ \beta_{YR,01} \\ \beta_{ZR,01} \end{bmatrix} + \begin{bmatrix} \beta_{XRG,max1}-\beta_{XRG,min1} \\ \beta_{YRG,max1}-\beta_{YRG,min1} \\ \beta_{ZRG,max1}-\beta_{ZRG,min1} \end{bmatrix} V_{Gref} + \begin{bmatrix} \beta_{XRB,max1}-\beta_{XRB,min1} \\ \beta_{YRB,max1}-\beta_{YRB,min1} \\ \beta_{ZRB,max1}-\beta_{ZRB,min1} \end{bmatrix} V_{Bref} \quad \text{for } 0 \le V_{Rref} \le 0.5 \quad (29a)$$

$$\begin{bmatrix} \beta_{XR2}\left(V_{Gref},V_{Bref}\right) \\ \beta_{YR2}\left(V_{Gref},V_{Bref}\right) \\ \beta_{ZR2}\left(V_{Gref},V_{Bref}\right) \end{bmatrix} = \begin{bmatrix} \beta_{XR,02} \\ \beta_{YR,02} \\ \beta_{ZR,02} \end{bmatrix} + \begin{bmatrix} \beta_{XRG,max2}-\beta_{XRG,min2} \\ \beta_{YRG,max2}-\beta_{YRG,min2} \\ \beta_{ZRG,max2}-\beta_{ZRG,min2} \end{bmatrix} V_{Gref} + \begin{bmatrix} \beta_{XRB,max2}-\beta_{XRB,min2} \\ \beta_{YRB,max2}-\beta_{YRB,min2} \\ \beta_{ZRB,max2}-\beta_{ZRB,min2} \end{bmatrix} V_{Bref} \quad \text{for } 0.5 < V_{Rref} \le 1 \quad (29b)$$

Likewise, the functions of γ_{XR1}, γ_{XR1}, γ_{YR1}, γ_{YR1}, γ_{ZR1}, and γ_{ZR1} can be written as

$$\begin{bmatrix} \gamma_{XR1}\left(V_{Gref},V_{Bref}\right) \\ \gamma_{YR1}\left(V_{Gref},V_{Bref}\right) \\ \gamma_{ZR1}\left(V_{Gref},V_{Bref}\right) \end{bmatrix} = \begin{bmatrix} \gamma_{XR,01} \\ \gamma_{YR,01} \\ \gamma_{ZR,01} \end{bmatrix} + \begin{bmatrix} \gamma_{XRG,max1}-\gamma_{XRG,min1} \\ \gamma_{YRG,max1}-\gamma_{YRG,min1} \\ \gamma_{ZRG,max1}-\gamma_{ZRG,min1} \end{bmatrix} V_{Gref} + \begin{bmatrix} \gamma_{XRB,max1}-\gamma_{XRB,min1} \\ \gamma_{YRB,max1}-\gamma_{YRB,min1} \\ \gamma_{ZRB,max1}-\gamma_{ZRB,min1} \end{bmatrix} V_{Bref} \quad \text{for } 0 \le V_{Rref} \le 0.5 \quad (30a)$$

$$\begin{bmatrix}\gamma_{XR2}\left(V_{Gref},V_{Bref}\right)\\ \gamma_{YR2}\left(V_{Gref},V_{Bref}\right)\\ \gamma_{ZR2}\left(V_{Gref},V_{Bref}\right)\end{bmatrix}=\begin{bmatrix}\gamma_{XR,02}\\ \gamma_{YR,02}\\ \gamma_{ZR,02}\end{bmatrix}+\begin{bmatrix}\gamma_{XRG,max2}-\gamma_{XRG,min2}\\ \gamma_{YRG,max2}-\gamma_{YRG,min2}\\ \gamma_{ZRG,max2}-\gamma_{ZRG,min2}\end{bmatrix}V_{Gref}$$
$$+\begin{bmatrix}\gamma_{XRB,max2}-\gamma_{XRB,min2}\\ \gamma_{YRB,max2}-\gamma_{YRB,min2}\\ \gamma_{ZRB,max2}-\gamma_{ZRB,min2}\end{bmatrix}V_{Bref}\quad \text{for } 0.5<V_{Rref}\le 1 \quad (30b)$$

By substituting (28), (29) and (30) into (24), the general expression of (X_R, Y_R, Z_R) can be obtained as follows.

$$\begin{bmatrix}X_R\\ Y_R\\ Z_R\end{bmatrix}=\left\{\begin{bmatrix}\alpha_{XR,01}\\ \alpha_{YR,01}\\ \alpha_{ZR,01}\end{bmatrix}+\begin{bmatrix}\alpha_{XRG,max1}-\alpha_{XRG,min1}\\ \alpha_{YRG,max1}-\alpha_{YRG,min1}\\ \alpha_{ZRG,max1}-\gamma_{ZRG,min1}\end{bmatrix}V_{Gref}+\begin{bmatrix}\alpha_{XRB,max1}-\alpha_{XRB,min1}\\ \alpha_{YRB,max1}-\alpha_{YRB,min1}\\ \gamma_{ZRB,max1}-\alpha_{ZRB,min1}\end{bmatrix}V_{Bref}\right\}V_{Rref}^{\,3}$$
$$+\left\{\begin{bmatrix}\beta_{XR,01}\\ \beta_{YR,01}\\ \beta_{ZR,01}\end{bmatrix}+\begin{bmatrix}\beta_{XRG,max1}-\beta_{XRG,min1}\\ \beta_{YRG,max1}-\beta_{YRG,min1}\\ \beta_{ZRG,max1}-\beta_{ZRG,min1}\end{bmatrix}V_{Gref}+\begin{bmatrix}\beta_{XRB,max1}-\beta_{XRB,min1}\\ \beta_{YRB,max1}-\beta_{YRB,min1}\\ \beta_{ZRB,max1}-\beta_{ZRB,min1}\end{bmatrix}V_{Bref}\right\}V_{Rref}^{\,2}$$
$$+\left\{\begin{bmatrix}\gamma_{XR,01}\\ \gamma_{YR,01}\\ \gamma_{ZR,01}\end{bmatrix}+\begin{bmatrix}\gamma_{XRG,max1}-\gamma_{XRG,min1}\\ \gamma_{YRG,max1}-\gamma_{YRG,min1}\\ \gamma_{ZRG,max1}-\gamma_{ZRG,min1}\end{bmatrix}V_{Gref}+\begin{bmatrix}\gamma_{XRB,max1}-\gamma_{XRB,min1}\\ \gamma_{YRB,max1}-\gamma_{YRB,min1}\\ \gamma_{ZRB,max1}-\gamma_{ZRB,min1}\end{bmatrix}V_{Bref}\right\}V_{Rref}$$
$$\text{for } 0\le V_{Rref}\le 0.5 \quad (31a)$$

$$\begin{bmatrix}X_R\\ Y_R\\ Z_R\end{bmatrix}=\left\{\begin{bmatrix}\alpha_{XR,02}\\ \alpha_{YR,02}\\ \alpha_{ZR,02}\end{bmatrix}+\begin{bmatrix}\alpha_{XRG,max2}-\alpha_{XRG,min2}\\ \alpha_{YRG,max2}-\alpha_{YRG,min2}\\ \alpha_{ZRG,max2}-\gamma_{ZRG,min2}\end{bmatrix}V_{Gref}+\begin{bmatrix}\alpha_{XRB,max2}-\alpha_{XRB,min2}\\ \alpha_{YRB,max2}-\alpha_{YRB,min2}\\ \alpha_{ZRB,max2}-\alpha_{ZRB,min2}\end{bmatrix}V_{Bref}\right\}V_{Rref}^{\,3}$$
$$+\left\{\begin{bmatrix}\beta_{XR,02}\\ \beta_{YR,02}\\ \beta_{ZR,02}\end{bmatrix}+\begin{bmatrix}\beta_{XRG,max2}-\beta_{XRG,min2}\\ \beta_{YRG,max2}-\beta_{YRG,min2}\\ \beta_{ZRG,max2}-\beta_{ZRG,min2}\end{bmatrix}V_{Gref}+\begin{bmatrix}\beta_{XRB,max2}-\beta_{XRB,min2}\\ \beta_{YRB,max2}-\beta_{YRB,min2}\\ \beta_{ZRB,max2}-\beta_{ZRB,min2}\end{bmatrix}V_{Bref}\right\}V_{Rref}^{\,2}$$
$$+\left\{\begin{bmatrix}\gamma_{XR,02}\\ \gamma_{YR,02}\\ \gamma_{ZR,02}\end{bmatrix}+\begin{bmatrix}\gamma_{XRG,max2}-\gamma_{XRG,min2}\\ \gamma_{YRG,max2}-\gamma_{YRG,min2}\\ \gamma_{ZRG,max2}-\gamma_{ZRG,min2}\end{bmatrix}V_{Gref}+\begin{bmatrix}\gamma_{XRB,max2}-\gamma_{XRB,min2}\\ \gamma_{YRB,max2}-\gamma_{YRB,min2}\\ \gamma_{ZRB,max2}-\gamma_{ZRB,min2}\end{bmatrix}V_{Bref}\right\}V_{Rref}$$
$$\text{for } 0.5<V_{Rref}\le 1 \quad (31b)$$

From the measurement results in Fig. 9, the numerical values of the parameters in (31a) and (31b) are obtained, as listed in Table II and III, respectively.

TABLE II. PARAMETER VALUES IN (27a) FOR RED LEDs.

$\alpha_{XR,01}$	$\alpha_{XRG,max1}$	$\alpha_{XRG,min1}$	$\alpha_{XRB,max1}$	$\alpha_{XRB,min1}$
0.35513	0.94109	0.355129	0.71865	0.35513
$\alpha_{YR,01}$	$\alpha_{YRG,max1}$	$\alpha_{YRG,min1}$	$\alpha_{YRB,max1}$	$\alpha_{YRB,min1}$
0.16320	0.41332	0.16320	0.71865	0.16320
$\alpha_{ZR,01}$	$\alpha_{ZRG,max1}$	$\alpha_{ZRG,min1}$	$\alpha_{ZRB,max1}$	$\alpha_{ZRB,min1}$
7.64×10^{-5}	0.00017	7.64×10^{-5}	0.000102	7.64×10^{-5}
$\beta_{XR,01}$	$\beta_{XRG,max1}$	$\beta_{XRG,min1}$	$\beta_{XRB,max1}$	$\beta_{XRB,min1}$
-1.25128	-1.17171	-1.25128	-1.47996	-1.25128
$\beta_{YR,01}$	$\beta_{YRG,max1}$	$\beta_{YRG,min1}$	$\beta_{YRB,max1}$	$\beta_{YRB,min1}$
-0.55003	-0.73933	-0.55003	-0.62847	-0.55003
$\beta_{ZR,01}$	$\beta_{ZRG,max1}$	$\beta_{ZRG,min1}$	$\beta_{ZRB,max1}$	$\beta_{ZRB,min1}$
-0.00021	-0.000267	-0.00021	-0.000195	-0.00021
$\gamma_{XR,01}$	$\gamma_{XRG,max1}$	$\gamma_{XRG,min1}$	$\gamma_{XRB,max1}$	$\gamma_{XRB,min1}$
1.25260	1.03126	1.25260	1.00079	1.25260
$\gamma_{YR,01}$	$\gamma_{YRG,max1}$	$\gamma_{YRG,min1}$	$\gamma_{YRB,max1}$	$\gamma_{YRB,min1}$
0.533984	0.43513	0.53398	0.41912	0.53398
$\gamma_{ZR,01}$	$\gamma_{ZRG,max1}$	$\gamma_{ZRG,min1}$	$\gamma_{ZRB,max1}$	$\gamma_{ZRB,min1}$
0.00017	0.000135	0.00017	1.19×10^{-4}	0.00017

TABLE III. PARAMETER VALUES IN (27b) FOR RED LEDs.

$\alpha_{XR,02}$	$\alpha_{XRG,max2}$	$\alpha_{XRG,min2}$	$\alpha_{XRB,max2}$	$\alpha_{XRB,min2}$
0.26895	0.24204	0.26895	0.43457	0.26895
$\alpha_{YR,02}$	$\alpha_{YRG,max2}$	$\alpha_{YRG,min2}$	$\alpha_{YRB,max2}$	$\alpha_{YRB,min2}$
0.12815	0.10632	0.12815	0.18639	0.12815
$\alpha_{ZR,02}$	$\alpha_{ZRG,max2}$	$\alpha_{ZRG,min2}$	$\alpha_{ZRB,max2}$	$\alpha_{ZRB,min2}$
6.93×10^{-5}	4.04×10^{-5}	6.93×10^{-5}	6.29×10^{-5}	6.93×10^{-5}
$\beta_{XR,02}$	$\beta_{XRG,max2}$	$\beta_{XRG,min2}$	$\beta_{XRB,max2}$	$\beta_{XRB,min2}$
-1.36598	-0.97479	-1.36598	-1.29553	-1.36598
$\beta_{YR,02}$	$\beta_{YRG,max2}$	$\beta_{YRG,min2}$	$\beta_{YRB,max2}$	$\beta_{YRB,min2}$
-0.60045	-0.41350	-0.60045	-0.54738	-0.60045
$\beta_{ZR,02}$	$\beta_{ZRG,max2}$	$\beta_{ZRG,min2}$	$\beta_{ZRB,max2}$	$\beta_{ZRB,min2}$
-0.00023	-1.29×10^{-4}	-0.00023	-1.67×10^{-4}	-2.31×10^{-4}
$\gamma_{XR,02}$	$\gamma_{XRG,max2}$	$\gamma_{XRG,min2}$	$\gamma_{XRB,max2}$	$\gamma_{XRB,min2}$
1.36151	0.83811	1.36151	0.99573	1.36151
$\gamma_{YR,02}$	$\gamma_{YRG,max2}$	$\gamma_{YRG,min2}$	$\gamma_{YRB,max2}$	$\gamma_{YRB,min2}$
0.58070	0.35043	0.58070	0.41583	0.58070
$\gamma_{ZR,02}$	$\gamma_{ZRG,max2}$	$\gamma_{ZRG,min2}$	$\gamma_{ZRB,max2}$	$\gamma_{ZRB,min2}$
1.88×10^{-4}	9.93×10^{-5}	1.88×10^{-4}	1.16×10^{-4}	1.88×10^{-4}

To best fit the measured tristimulus values (X_G, Y_G, Z_G) and (X_B, Y_B, Z_B) of the green and blue LED sources [see Fig. 10 and Fig. 11], second-order polynomial functions are used. By employing similar interpolation method, the general expressions of (X_G, Y_G, Z_G) and (X_B, Y_B, Z_B) are obtained in (32) and (33), respectively. Table IV and V contain the corresponding parameter values.

$$\begin{bmatrix}X_G\\ Y_G\\ Z_G\end{bmatrix}=\left\{\begin{bmatrix}\alpha_{XG,0}\\ \alpha_{YG,0}\\ \alpha_{ZG,0}\end{bmatrix}+\begin{bmatrix}\alpha_{XGR,max}-\alpha_{XGR,min}\\ \alpha_{YGR,max}-\alpha_{YGR,min}\\ \alpha_{ZGR,max}-\alpha_{ZGR,min}\end{bmatrix}V_{Rref}+\begin{bmatrix}\alpha_{XGB,max}-\alpha_{XGB,min}\\ \alpha_{YGB,max}-\alpha_{YGB,min}\\ \alpha_{ZGB,max}-\alpha_{ZGB,min}\end{bmatrix}V_{Bref}\right\}V_{Gref}^{\,2}$$
$$+\left\{\begin{bmatrix}\beta_{XG,0}\\ \beta_{YG,0}\\ \beta_{ZG,0}\end{bmatrix}+\begin{bmatrix}\beta_{XGR,max}-\beta_{XGR,min}\\ \beta_{YGR,max}-\beta_{YGR,min}\\ \beta_{ZGR,max}-\beta_{ZGR,min}\end{bmatrix}V_{Rref}+\begin{bmatrix}\beta_{XGB,max}-\beta_{XGB,min}\\ \beta_{YGB,max}-\beta_{YGB,min}\\ \beta_{ZGB,max}-\beta_{ZGB,min}\end{bmatrix}V_{Bref}\right\}V_{Gref} \quad (32)$$

$$\begin{bmatrix}X_B\\ Y_B\\ Z_B\end{bmatrix}=\left\{\begin{bmatrix}\alpha_{XB,0}\\ \alpha_{YB,0}\\ \alpha_{ZB,0}\end{bmatrix}+\begin{bmatrix}\alpha_{XBR,max}-\alpha_{XBR,min}\\ \alpha_{YBR,max}-\alpha_{YBR,min}\\ \alpha_{ZBR,max}-\alpha_{ZBR,min}\end{bmatrix}V_{Rref}+\begin{bmatrix}\alpha_{XBG,max}-\alpha_{XBG,min}\\ \alpha_{YBG,max}-\alpha_{YBG,min}\\ \alpha_{ZBG,max}-\alpha_{ZBG,min}\end{bmatrix}V_{Gref}\right\}V_{Bref}^{\,2}$$
$$+\left\{\begin{bmatrix}\beta_{XB,0}\\ \beta_{YB,0}\\ \beta_{ZB,0}\end{bmatrix}+\begin{bmatrix}\beta_{XBR,max}-\beta_{XBR,min}\\ \beta_{YBR,max}-\beta_{YBR,min}\\ \beta_{ZBR,max}-\beta_{ZBR,min}\end{bmatrix}V_{Rref}+\begin{bmatrix}\beta_{XBG,max}-\beta_{XBG,min}\\ \beta_{YBG,max}-\beta_{YBG,min}\\ \beta_{ZBG,max}-\beta_{ZBG,min}\end{bmatrix}V_{Gref}\right\}V_{Bref} \quad (33)$$

TABLE IV. PARAMETER VALUES IN (28) FOR GREEN LEDs.

$\alpha_{XG,0}$	$\alpha_{XGR,max}$	$\alpha_{XGR,min}$	$\alpha_{XGB,max}$	$\alpha_{XGB,min}$
-0.12711	-0.13931	-0.12711	-0.15163	-0.12711
$\alpha_{YG,0}$	$\alpha_{YGR,max}$	$\alpha_{YGR,min}$	$\alpha_{YGB,max}$	$\alpha_{YGB,min}$
-0.49553	-0.45918	-0.49553	-0.53569	-0.49553
$\alpha_{ZG,0}$	$\alpha_{ZGR,max}$	$\alpha_{ZGR,min}$	$\alpha_{ZGB,max}$	$\alpha_{ZGB,min}$
-0.04168	-0.00322	-0.04168	-0.03299	-0.04168
$\beta_{XG,0}$	$\beta_{XGR,max}$	$\beta_{XGR,min}$	$\beta_{XGB,max}$	$\beta_{XGB,min}$
0.29714	0.31134	0.29714	0.31878	0.29714
$\beta_{YG,0}$	$\beta_{YGR,max}$	$\beta_{YGR,min}$	$\beta_{YGB,max}$	$\beta_{YGB,min}$
1.17687	1.06814	1.17687	1.10570	1.17687
$\beta_{ZG,0}$	$\beta_{ZGR,max}$	$\beta_{ZGR,min}$	$\beta_{ZGB,max}$	$\beta_{ZGB,min}$
0.15970	0.08736	0.15970	0.07014	0.15970

TABLE V. PARAMETER VALUES IN (29) FOR BLUE LEDs.

$\alpha_{XB,0}$	$\alpha_{XBR,max}$	$\alpha_{XBR,min}$	$\alpha_{XBG,max}$	$\alpha_{XBG,min}$
0.01	-0.01052	0.01	0.00980	0.01
$\alpha_{YB,0}$	$\alpha_{YBR,max}$	$\alpha_{YBR,min}$	$\alpha_{YBG,max}$	$\alpha_{YBG,min}$
-0.01664	-0.05178	-0.01664	0.01413	-0.01664
$\alpha_{ZB,0}$	$\alpha_{ZBR,max}$	$\alpha_{ZBR,min}$	$\alpha_{ZBG,max}$	$\alpha_{ZBG,min}$
-0.00725	-0.13676	-0.00725	0.03833	-0.00725
$\beta_{XB,0}$	$\beta_{XBR,max}$	$\beta_{XBR,min}$	$\beta_{XBG,max}$	$\beta_{XBG,min}$
0.15125	0.15034	0.15125	0.13231	0.15125
$\beta_{YB,0}$	$\beta_{YBR,max}$	$\beta_{YBR,min}$	$\beta_{YBG,max}$	$\beta_{YBG,min}$
0.25855	0.30190	0.25855	0.21266	0.25855
$\beta_{ZB,0}$	$\beta_{ZBR,max}$	$\beta_{ZBR,min}$	$\beta_{ZBG,max}$	$\beta_{ZBG,min}$
1.16734	1.18728	1.16734	1.02041	1.16734

The total tristimulus values (X_T, Y_T, Z_T) of the closed-loop RGB system is the superposition (sum) of the tristimulus values of red, blue and green LED sources, which can be obtained by adding Equation (31)–(33). By entering the parameter values of Table II–V into (31)–(33), we can write

$$\begin{bmatrix} X_T \\ Y_T \\ Z_T \end{bmatrix} = \begin{bmatrix} X_R \\ Y_R \\ Z_R \end{bmatrix} + \begin{bmatrix} X_G \\ Y_G \\ Z_G \end{bmatrix} + \begin{bmatrix} X_B \\ Y_B \\ Z_B \end{bmatrix}$$

$$= \left\{ \begin{bmatrix} \alpha_{XR,01} \\ \alpha_{YR,01} \\ \alpha_{ZR,01} \end{bmatrix} + \begin{bmatrix} \alpha_{XRG1} \\ \alpha_{YRG1} \\ \alpha_{ZRG1} \end{bmatrix} V_{Gref} + \begin{bmatrix} \alpha_{XRB1} \\ \alpha_{YRB1} \\ \alpha_{ZRB1} \end{bmatrix} V_{Bref} \right\} V_{Rref}^3$$

$$+ \left\{ \begin{bmatrix} \beta_{XR,01} \\ \beta_{YR,01} \\ \beta_{ZR,01} \end{bmatrix} + \begin{bmatrix} \beta_{XRG1} \\ \beta_{YRG1} \\ \beta_{ZRG1} \end{bmatrix} V_{Gref} + \begin{bmatrix} \beta_{XRB1} \\ \beta_{YRB1} \\ \beta_{ZRB1} \end{bmatrix} V_{Bref} \right\} V_{Rref}^2$$

$$+ \left\{ \begin{bmatrix} \gamma_{XR,01} \\ \gamma_{YR,01} \\ \gamma_{ZR,01} \end{bmatrix} + \begin{bmatrix} \gamma_{XRG1} \\ \gamma_{YRG1} \\ \gamma_{ZRG1} \end{bmatrix} V_{Gref} + \begin{bmatrix} \gamma_{XRB1} \\ \gamma_{YRB1} \\ \gamma_{ZRB1} \end{bmatrix} V_{Bref} \right\} V_{Rref}$$

$$+ \left\{ \begin{bmatrix} \alpha_{XG,0} \\ \alpha_{YG,0} \\ \alpha_{ZG,0} \end{bmatrix} + \begin{bmatrix} \alpha_{XGR} \\ \alpha_{YGR} \\ \alpha_{ZGR} \end{bmatrix} V_{Rref} + \begin{bmatrix} \alpha_{XGB} \\ \alpha_{YGB} \\ \alpha_{ZGB} \end{bmatrix} V_{Bref} \right\} V_{Gref}^2$$

$$+ \left\{ \begin{bmatrix} \beta_{XG,0} \\ \beta_{YG,0} \\ \beta_{ZG,0} \end{bmatrix} + \begin{bmatrix} \beta_{XGR} \\ \beta_{YGR} \\ \beta_{ZGR} \end{bmatrix} V_{Rref} + \begin{bmatrix} \beta_{XGB} \\ \beta_{YGB} \\ \beta_{ZGB} \end{bmatrix} V_{Bref} \right\} V_{Gref}$$

$$+ \left\{ \begin{bmatrix} \alpha_{XB,0} \\ \alpha_{YB,0} \\ \alpha_{ZB,0} \end{bmatrix} + \begin{bmatrix} \alpha_{XBR} \\ \alpha_{YBR} \\ \alpha_{ZBR} \end{bmatrix} V_{Rref} + \begin{bmatrix} \alpha_{XBG} \\ \alpha_{YBG} \\ \alpha_{ZBG} \end{bmatrix} V_{Gref} \right\} V_{Bref}^2$$

$$+ \left\{ \begin{bmatrix} \beta_{XB,0} \\ \beta_{YB,0} \\ \beta_{ZB,0} \end{bmatrix} + \begin{bmatrix} \beta_{XBR} \\ \beta_{YBR} \\ \beta_{ZBR} \end{bmatrix} V_{Rref} + \begin{bmatrix} \beta_{XBG} \\ \beta_{YBG} \\ \beta_{ZBG} \end{bmatrix} V_{Gref} \right\} V_{Bref}$$

for $0 \le V_{Rref} \le 0.5$ (34a)

$$\begin{bmatrix} X_T \\ Y_T \\ Z_T \end{bmatrix} = \begin{bmatrix} X_R \\ Y_R \\ Z_R \end{bmatrix} + \begin{bmatrix} X_G \\ Y_G \\ Z_G \end{bmatrix} + \begin{bmatrix} X_B \\ Y_B \\ Z_B \end{bmatrix}$$

$$= \left\{ \begin{bmatrix} \alpha_{XR,02} \\ \alpha_{YR,02} \\ \alpha_{ZR,02} \end{bmatrix} + \begin{bmatrix} \alpha_{XRG2} \\ \alpha_{YRG2} \\ \alpha_{ZRG2} \end{bmatrix} V_{Gref} + \begin{bmatrix} \alpha_{XRB2} \\ \alpha_{YRB2} \\ \alpha_{ZRB2} \end{bmatrix} V_{Bref} \right\} V_{Rref}^3$$

$$+ \left\{ \begin{bmatrix} \beta_{XR,02} \\ \beta_{YR,02} \\ \beta_{ZR,02} \end{bmatrix} + \begin{bmatrix} \beta_{XRG2} \\ \beta_{YRG2} \\ \beta_{ZRG2} \end{bmatrix} V_{Gref} + \begin{bmatrix} \beta_{XRB2} \\ \beta_{YRB2} \\ \beta_{ZRB2} \end{bmatrix} V_{Bref} \right\} V_{Rref}^2$$

$$+ \left\{ \begin{bmatrix} \gamma_{XR,02} \\ \gamma_{YR,02} \\ \gamma_{ZR,02} \end{bmatrix} + \begin{bmatrix} \gamma_{XRG2} \\ \gamma_{YRG2} \\ \gamma_{ZRG2} \end{bmatrix} V_{Gref} + \begin{bmatrix} \gamma_{XRB2} \\ \gamma_{YRB2} \\ \gamma_{ZRB2} \end{bmatrix} V_{Bref} \right\} V_{Rref}$$

$$+ \left\{ \begin{bmatrix} \alpha_{XG,0} \\ \alpha_{YG,0} \\ \alpha_{ZG,0} \end{bmatrix} + \begin{bmatrix} \alpha_{XGR} \\ \alpha_{YGR} \\ \alpha_{ZGR} \end{bmatrix} V_{Rref} + \begin{bmatrix} \alpha_{XGB} \\ \alpha_{YGB} \\ \alpha_{ZGB} \end{bmatrix} V_{Bref} \right\} V_{Gref}^2$$

$$+ \left\{ \begin{bmatrix} \beta_{XG,0} \\ \beta_{YG,0} \\ \beta_{ZG,0} \end{bmatrix} + \begin{bmatrix} \beta_{XGR} \\ \beta_{YGR} \\ \beta_{ZGR} \end{bmatrix} V_{Rref} + \begin{bmatrix} \beta_{XGB} \\ \beta_{YGB} \\ \beta_{ZGB} \end{bmatrix} V_{Bref} \right\} V_{Gref}$$

$$+ \left\{ \begin{bmatrix} \alpha_{XB,0} \\ \alpha_{YB,0} \\ \alpha_{ZB,0} \end{bmatrix} + \begin{bmatrix} \alpha_{XBR} \\ \alpha_{YBR} \\ \alpha_{ZBR} \end{bmatrix} V_{Rref} + \begin{bmatrix} \alpha_{XBG} \\ \alpha_{YBG} \\ \alpha_{ZBG} \end{bmatrix} V_{Gref} \right\} V_{Bref}^2$$

$$+ \left\{ \begin{bmatrix} \beta_{XB,0} \\ \beta_{YB,0} \\ \beta_{ZB,0} \end{bmatrix} + \begin{bmatrix} \beta_{XBR} \\ \beta_{YBR} \\ \beta_{ZBR} \end{bmatrix} V_{Rref} + \begin{bmatrix} \beta_{XBG} \\ \beta_{YBG} \\ \beta_{ZBG} \end{bmatrix} V_{Gref} \right\} V_{Bref}$$

for $0.5 < V_{Rref} \le 1$ (34b)

TABLE VI. PARAMETER VALUES IN (34a) AND (34b).

α_{XRG1}	α_{XRB1}	α_{XRG2}	α_{XRB2}
0.58596	0.36352	-0.02691	0.16562
α_{YRG1}	α_{YRB1}	α_{YRG2}	α_{YRB2}
0.25012	0.55545	-0.02183	0.05824
α_{ZRG1}	α_{ZRB1}	α_{ZRG2}	α_{ZRB2}
9.36×10^{-5}	2.56×10^{-5}	-2.89×10^{-5}	-6.4×10^{-6}
β_{XRG1}	β_{XRB1}	β_{XRG2}	β_{XRB2}
0.07957	-0.22868	0.39119	0.07045
β_{YRG1}	β_{YRB1}	β_{YRG2}	β_{YRB2}
-0.1893	-0.07844	0.18695	0.05307
β_{ZRG1}	β_{ZRB1}	β_{ZRG2}	β_{ZRB2}
-5.7×10^{-5}	1.5×10^{-5}	1.01×10^{-4}	6.4×10^{-5}
γ_{XRG1}	γ_{XRB1}	γ_{XRG2}	γ_{XRB2}
-0.22134	-0.25181	-0.5234	-0.36578
γ_{YRG1}	γ_{YRB1}	γ_{YRG2}	γ_{YRB2}
-0.09885	-0.11486	-0.23027	-0.16487
γ_{ZRG1}	γ_{ZRB1}	γ_{ZRG2}	γ_{ZRB2}
-3.5×10^{-5}	-5.1×10^{-5}	-8.87×10^{-5}	-7.2×10^{-5}
α_{XGR}	α_{XGB}	α_{XBR}	α_{XBG}
-0.0122	-0.02452	-0.02052	-2×10^{-4}
α_{YGR}	α_{YGB}	α_{YBR}	α_{YBG}
0.03635	-0.04016	-0.03514	0.03077
α_{ZGR}	α_{ZGB}	α_{ZBR}	α_{ZBG}
0.03846	8.69×10^{-3}	-0.12951	0.04558
β_{XGR}	β_{XGB}	β_{XBR}	β_{XBG}
0.0142	0.02164	-9.1×10^{-4}	-0.01894
β_{YGR}	β_{YGB}	β_{YBR}	β_{YBG}
-0.10873	-0.07117	0.04335	-0.04589
β_{ZGR}	β_{ZGB}	β_{ZBR}	β_{ZBG}
-0.07234	-0.08956	0.01994	-0.14693

Note that the remaining parameter values in (34a) and (34b), e.g. $\alpha_{XR,01}$, $\alpha_{YR,01}$, $\alpha_{ZR,01}$, $\alpha_{XR,02}$, $\alpha_{YR,02}$ and $\alpha_{ZR,02}$, are already listed in Table II–V and are not replicated in Table VI.

IV. Experimental Results

A photograph of the hardware prototype of the DC-DC SITO buck LED driver is shown in Fig. 12.

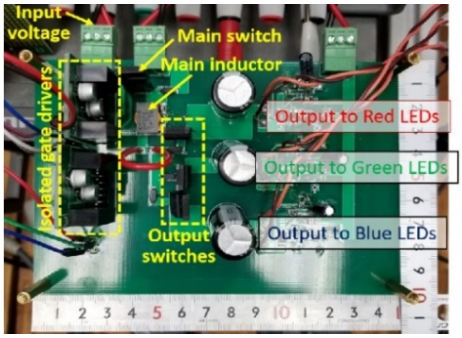

Fig. 12. Photograph of the DC-DC SITO buck LED driver.

Table VII shows the design specifications while the part numbers of the key components are listed in Table VIII. Fig. 13 shows the entire experimental setup.

TABLE VII. DESIGN SPECIFICATIONS.

Parameter	Value
Input voltage	24 V
Main inductor	3 μH
Output capacitor per string	1 mF
Switching frequency of main switch	150 kHz
Current sense resistor	100 mΩ
LED current range per string	50–550 mA
Typical forward current per red LED	350 mA
Typical forward voltage per red LED	2.9 V
Typical forward current per green LED	350 mA
Typical forward voltage per green LED	3.21 V
Typical forward current per blue LED	350 mA
Typical forward voltage per blue LED	2.95 V
Total number of red LEDs used	4
Total number of green LEDs used	4
Total number blue LEDs used	4

TABLE VIII. LIST OF KEY COMPONENTS.

Component	Part number
Power MOSFET	Infineon IPA083N10N5
Gate driver	ADUM3223ARZ
Main inductor	EPCOS (TDK) B82559A0302A013
Schottky diode	Comchip Technology CDBA240LL-G
Current sense resistor	Vishay Dale WSLT2512R1000FEA
Operational amplifier	OPA354
Microcontroller (MCU)	TMS320F28335
Red LED chip	Lumiled LXML-PD01-0050
Green LED chip	Lumiled LXML-PM01-0090
Blue LED chip	Lumiled LXML-PB01-0040

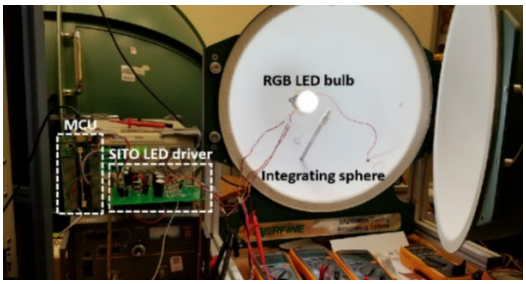

Fig. 13. Experimental setup of the closed-loop RGB LED system.

Due to the inherent nature of the time-multiplexing control scheme of the SITO LED driver, the discharging time interval of the output capacitor dominates a full cycle per output, where a full cycle is 1/50 kHz (or 20 μs). Hence, a larger output capacitor helps reduce the output voltage (or current) ripple. Besides, an LED device under forward bias exhibits an exponential I-V relationship, which means that a small change in the LED voltage will lead to a larger change in the LED current. Such current variation will become the largest when the forward current reaches its maximum value of 550 mA for the specified target current range of 50 mA–550 mA. Thus, we set a stringent condition of 1% LED current ripple at the "worst-case" operating point of 550 mA. Based on this design constraint, the minimum value of the output capacitor can be determined by using equation (35). In short, (35) is derived by using the equivalent circuit diagram of a particular output of the SITO LED driver whereby the inductor current is zero (or the corresponding output switch is switched OFF).

$$C_o \geq \frac{V_o}{R_{LED}\left(\left|\frac{\Delta V_o}{\Delta t}\right| + R_{ESR}\left|\frac{\Delta I_o}{\Delta t}\right|\right)} \tag{35}$$

where V_o is the output voltage, R_{LED} is the equivalent resistance of the LED string, R_{ESR} is the equivalent series resistance (ESR) of the output capacitor, ΔV_o is the reduction of the output voltage, ΔI_o is the reduction of the output (LED) current, and Δt is the discharging time interval of the output capacitor.

From the I-V curve of the chosen blue LED, a 0.1% change in the forward voltage (V_F) results in a 1% change in the forward current (I_F). For the blue LED string, when I_F = 550 mA, V_o = 11.57 V. ΔV_o = 0.1% × 11.57 V = 11.57 mV. ΔI_o = 1% × 550 mA = 5.5 mA. R_{ESR} is assume to be 60 mΩ. The simulation results show that $\Delta t \approx 16.62$ μs. By substituting these values into (35), $C_o \geq 771$ μF. Since most electrolytic capacitor (E-cap) have a ±20% tolerance, the minimum value of C_o is determined to be 771 μF × 1.1 ≈ 848 μF. The commercially-available E-cap with a rated voltage of 25 V manufactured by, say EPCOS-TDK Electronics, whose value is nearest to and greater than 848 μF is 1000 μF (or 1 mF). Hence, 1 mF output capacitor is used for the blue LED string. The above analysis is repeated for the green and red LED string. For the green LED string, the minimum value of C_o is determined to be 816 μF. Likewise, for the red LED string, the minimum value of C_o is determined to be 732 μF. Either 820 μF or 1 mF standard E-cap can be used. But since 1 mF E-caps are already available in our lab, it is also used as the output capacitor for the green and red LED strings.

To start with, the preciseness of our current regulation is experimentally verified. In view of the errors in the current-sensing circuit and digital control, the measured value of the LED current in each string is compared to the corresponding expected (target) value, as shown in Table IX. Normalized reference voltages are provided for ease of comparison.

TABLE IX. COMPARISON BETWEEN MEASURED AND EXPECTED LED CURRENT VALUES.

Exp. current (mA)	Meas. I_R (mA)	Meas. I_G (mA)	Meas. I_B (mA)	Norm. V_{Rref} (V)	Norm. V_{Gref} (V)	Norm. V_{Bref} (V)
50	51	49	46	0.07	0.10	0.14
100	98	95	97	0.15	0.18	0.22
150	150	146	146	0.24	0.27	0.31
200	199	197	196	0.33	0.36	0.39
250	248	245	246	0.43	0.45	0.47
300	297	295	295	0.52	0.54	0.56
350	351	352	352	0.62	0.64	0.65
400	401	400	399	0.71	0.73	0.74
450	453	446	452	0.81	0.80	0.82
500	504	505	504	0.91	0.91	0.92
550	551	556	555	1.00	1.00	1.00

The experimental results show that the average error between the expected current and the actual current is only 1.478% and

the maximum error is 8% (when the expected current is 50 mA and the measured I_B = 46 mA). It shows that within the specified range of LED current (50–550 mA), the closed-loop control is capable of achieving a reasonably precise current regulation, albeit the errors generated by the circuit sensing circuitry.

To further study how the accuracy of the closed-loop current control of the SITO LED driver will ultimately affect the optical performance, six different sets of optical measurements are performed at different times. In each set, six separate tests are conducted. For example, the first two tests (Test 1 and 2) are performed in the afternoon and evening of the first day. The next two tests (Test 3 and 4) are performed in the afternoon and evening of the second day, etc. The objective is to verify the consistency and accuracy of the measured optical parameters across different combinations of the reference voltages (or LED current levels) and different times. In particular, it is crucial to verify how the current fluctuations will affect the optical parameters such as luminous flux and color coordinates. Table X to XIV show the experimental results with different combinations of target LED currents (I_R, I_G, I_B) across the three strings. The target current values are listed in the table caption.

TABLE X. MEASURED VALUES OF LUMINOUS FLUX AND COLOR COORDINATES WITH TARGET CURRENT VALUES OF (I_R, I_G, I_B) = (130 mA, 280 mA, 435 mA).

	Meas. I_R (mA)	Meas. I_G (mA)	Meas. I_B (mA)	Lum. Flux (lm)	x-coord.	y-coord.
TEST 1	133	281	441	470.53	0.1852	0.342
TEST 2	129	275	434	471.16	0.1855	0.3416
TEST 3	129	275	435	473.06	0.1857	0.3412
TEST 4	129	276	436	471.64	0.1849	0.3415
TEST 5	129	276	435	472.42	0.1855	0.3412
TEST 6	130	276	435	472.25	0.1854	0.3423

TABLE XI. MEASURED VALUES OF LUMINOUS FLUX AND COLOR COORDINATES WITH TARGET CURRENT VALUES OF (I_R, I_G, I_B) = (290, 445 mA, 50 mA).

	Meas. I_R (mA)	Meas. I_G (mA)	Meas. I_B (mA)	Lum. Flux (lm)	x-coord.	y-coord.
TEST 1	286	440	52	479.98	0.3105	0.5473
TEST 2	286	441	53	478.66	0.3085	0.5464
TEST 3	286	441	53	479.01	0.3088	0.5463
TEST 4	286	441	53	479.36	0.3089	0.5462
TEST 5	286	440	52	477.43	0.309	0.5479
TEST 6	286	441	53	481.26	0.3105	0.5467

TABLE XII. MEASURED VALUES OF LUMINOUS FLUX AND COLOR COORDINATES WITH TARGET CURRENT VALUES OF (I_R, I_G, I_B) = (445 mA, 110 mA, 255 mA).

	Meas. I_R (mA)	Meas. I_G (mA)	Meas. I_B (mA)	Lum. Flux (lm)	x-coord.	y-coord.
TEST 1	444	109	253	305.59	0.2676	0.3218
TEST 2	444	110	253	304.09	0.264	0.3223
TEST 3	443	109	254	303.77	0.2644	0.3218
TEST 4	444	110	253	303.95	0.264	0.3215
TEST 5	444	110	253	305.59	0.2651	0.3226
TEST 6	444	109	253	304.81	0.2656	0.3222

TABLE XIII. MEASURED VALUES OF LUMINOUS FLUX AND COLOR COORDINATES WITH TARGET CURRENT VALUES OF (I_R, I_G, I_B) = (400 mA, 400 mA, 400 mA).

	Meas. I_R (mA)	Meas. I_G (mA)	Meas. I_B (mA)	Lum. Flux (lm)	x-coord.	y-coord.
TEST 1	401	400	399	543.31	0.2022	0.3824
TEST 2	400	400	399	544.08	0.2027	0.3819
TEST 3	400	400	399	538.54	0.1996	0.3826
TEST 4	400	400	399	541.93	0.2015	0.3814
TEST 5	400	399	398	543.22	0.2025	0.383
TEST 6	400	399	399	543.74	0.2025	0.3833

TABLE XIV. MEASURED VALUES OF LUMINOUS FLUX AND COLOR COORDINATES WITH TARGET CURRENT VALUES OF (I_R, I_G, I_B) = (50 mA, 50 mA, 50 mA).

	Meas. I_R (mA)	Meas. I_G (mA)	Meas. I_B (mA)	Lum. Flux (lm)	x-coord.	y-coord.
TEST 1	52	49	46	122.25	0.3012	0.4351
TEST 2	52	49	46	122.35	0.301	0.4348
TEST 3	51	48	46	120.30	0.3018	0.4359
TEST 4	51	48	46	120.27	0.3019	0.4352
TEST 5	51	48	46	120.02	0.3016	0.4356
TEST 6	52	50	46	123.01	0.3023	0.4345

To summarize, the measured DC value of each LED string is within ±5 mA when compared with the corresponding target current. This means that the measured currents are in close agreement with the corresponding target currents, thereby confirming that the current regulation is consistent and accurate. Using the data in Test 1 as the golden reference, the average error of luminous flux is only 0.32%. The average error of the x-coordinate is 0.54% while that of the y-coordinate is 0.15%. In particular, from Table IX, it is observed that the maximum current error of 8% is produced when the LED current is at its minimum value (i.e. $I_R = I_G = I_B$ = 50 mA). So, we measured the luminous flux and color points at the minimum current value. From the measured data in Table XIV, the percentage errors of luminous flux and color coordinates are very small. In this case, the maximum percentage error of luminous flux is 1.82% while the maximum percentage errors of the x- and y-coordinates are only 0.3023% and 0.18%, respectively. The experimental results show that the measured optical parameters are fairly consistent across different current values and different times. In short, the errors generated by the current sensing circuit when the SITO LED driver operates within the target current range (50–550 mA) are shown to be reasonably small. Hence, the circuit errors are not significant enough to affect the luminous flux and color point of the RGB LED system.

To experimentally verify the hardware prototype of the SITO LED driver, the key signals such as the inductor current (I_L), the red, green and blue LED currents (I_R, I_G, I_B) along with the gate drive signals of the main switch (S_{main}) and the output switches (S_1, S_2, S_3) are measured. Fig. 14 shows the measured current waveforms of I_L, I_R, I_G and I_B. Fig. 15 shows the measured waveforms of the gate drive signals of S_{main}, S_1, S_2 and S_3.

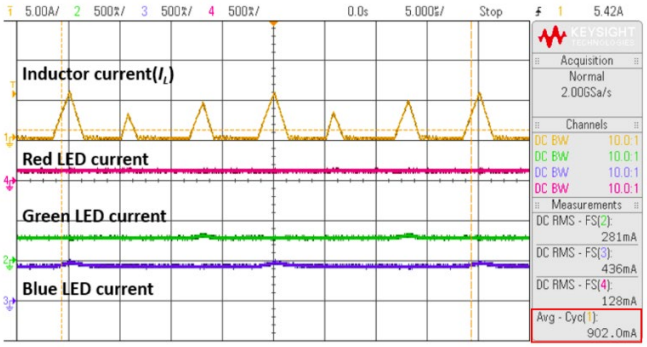

Fig. 14. Measured waveforms of the inductor current and the red, green and blue LED current.

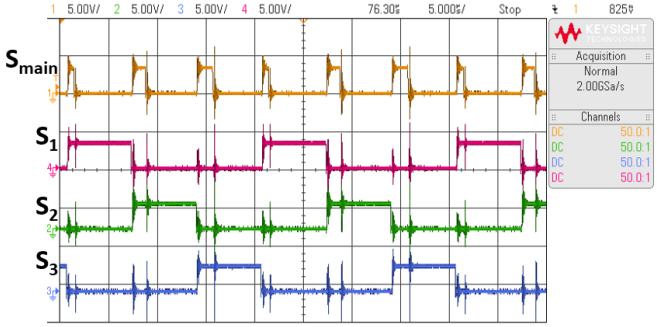

Fig. 15. Measured waveforms of the gate drive signals of the main switch and the three output switches.

Fig. 14 shows that the inductor current returns to zero before the end of each switching cycle, which indicates that SITO LED driver operates in discontinuous conduction mode (DCM). It also shows an uneven distribution of the peak values of the inductor current. This is attributed to *unequal* current levels across the three LED strings. In this unbalanced load current condition, the red LED string carries the smallest current of 129.3 mA whereas the blue LED carries the largest current of 432.9 mA. The on-time duty ratio of S_{main} pertaining to the red LED string is the smallest, which leads to the lowest peak value of the inductor current. Conversely, the on-time duty ratio of S_{main} pertaining to blue LED string is the largest, which results in the highest peak value of the inductor current.

Under the time-multiplexing control scheme, the energy stored in the inductor is successively transferred to each output channel in a round-robin, time-multiplexing manner. This means that only one output is enabled in each switching cycle. To eliminate cross-current conduction (or cross-regulation) issue across the three outputs, we need to make sure that the SITO LED driver stays in discontinuous conduction mode (DCM) at all times so that each LED string is fully decoupled in time. By definition, cross-regulation means a change in one output causes an unwanted change in another output, which is a common issue of SIMO-based converter. Additional experiments are conducted to study this issue. Fig. 16 shows an increase in the current of the red LED string from 130 mA to 400 mA. This is achieved by increasing the reference voltage of the red LED from 0.2 V to 0.71 V (both are normalized values). It shows that despite the load transient in red LED string, the current levels in the green and blue LED strings remain unchanged.

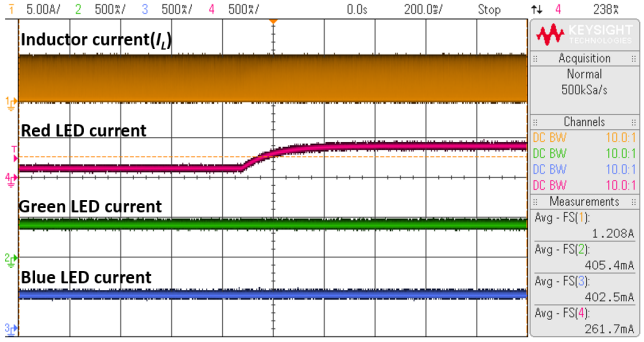

Fig. 16. Measured waveforms of the inductor current and the LED currents when red LED current increases from 130 mA to 400 mA.

Likewise, Fig. 17 shows the opposite scenario when the current in the red LED string is reduced from 400 mA to 130 mA. The experimental results show that the current levels of green and blue LED strings remain unaffected despite the load transient in the red LED string. Hence, the experimental results confirm that there is no noticeable cross-regulation.

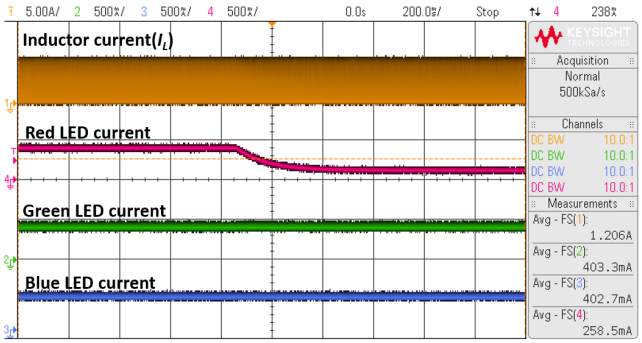

Fig. 17. Measured waveforms of the inductor current and the LED currents when red LED current decreases from 400 mA to 130 mA.

To experimentally verify the nonlinear empirical flux model, a wide range of reference voltage values (V_{Rref}, V_{Gref}, V_{Bref}) are chosen to perform the flux measurement. The resulting emitted light from the RGB LED light bulb is measured by the PMS-50 Spectrophotocolorimeter [28], as depicted in Fig. 18.

Fig. 18 compares the measured flux with the calculated flux from the empirical model for the same set of reference voltage values. The experimental results show that the maximum percentage error between the measured and calculated flux values is around 8.35%. The average percentage error between the measured and calculated flux values is only 2.98%. In addition, the proposed color model is validated by comparing the measured and calculated (x, y) color coordinates. For example, the value of V_{Bref} is swept by keeping (V_{Rref}, V_{Gref}) constant at either (0.2 V, 0.4 V) or (0.4 V, 0.2 V).

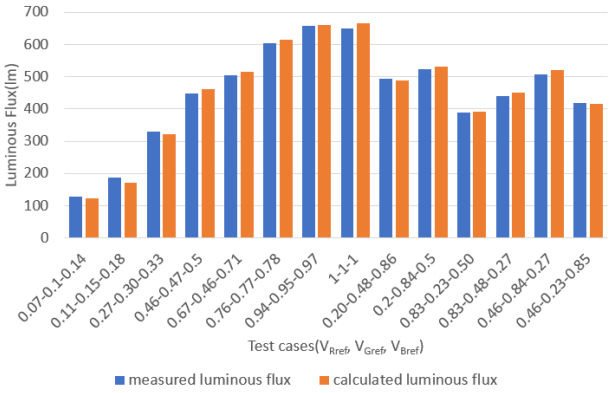

Fig. 18. Comparison of measured flux with calculated flux.

Fig. 19 compares the measured and calculated x and y values across different values of V_{Bref}. First, the total tristimulus values (X_T, Y_T, Z_T) are measured, which are then mapped into CIE 1931 color space in terms of (x, y) color coordinates by using (14). The maximum percentage error between measured and calculated x value (or y value) is 4.93% (or 7.28%). The average percentage error between the measured and calculated x value (or y value) is 3.87% (or 2.05%). The experimental results show that the proposed color model offers highly accurate and effective color control.

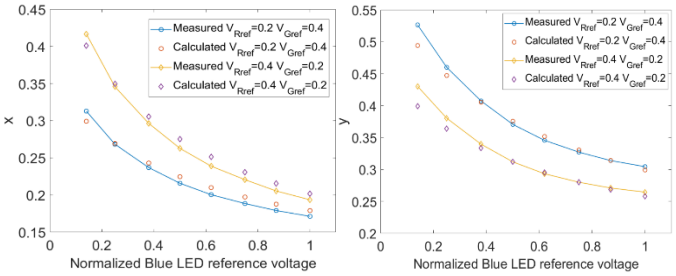

Fig. 19. Comparison of measured and calculated x and y values across different values of V_{Bref}.

Besides, we would like to compare the measured and calculated correlated color temperature (CCT) values across different values of V_{Bref}. In general, the following McCamy's formula is used to obtain the calculated CCT values from the chromaticity coordinates.

$$\mathrm{CCT} = 449n^3 + 3525n^2 + 6823.3n + 5520.33 \qquad (35)$$

where $n = (x - 0.3320) / (0.1858 - y)$.

The experimental measurements of CCT are carried out by using the PMS-50 Spectrophotocolorimeter and the integrating sphere. The value of V_{Bref} is swept from 0.14 V to 0.18 V while the values of V_{Rref} and V_{Gref} are fixed at 0.2 V and 0.1 V, respectively. From a practical standpoint, the CCT is tested within a range of 2000 K and 7500 K. The experimental results show that the average percentage error between the measured and calculated CCT values is 2.85%. The maximum percentage error between the measured and calculated CCT values is 4.39%, which are well within the maximum allowable CCT tolerance specified in [30]. Fig. 20 compares the measured and calculated CCT values across different values of V_{Bref}.

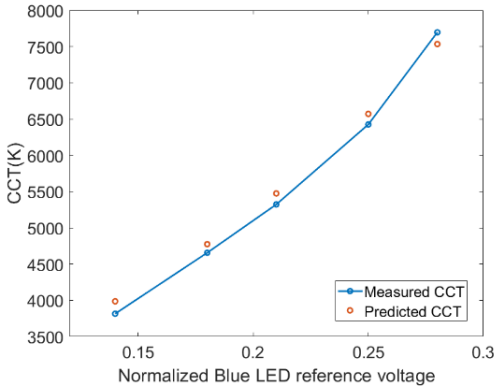

Fig. 20. Comparison between measured and calculated CCT values.

VI. Conclusions

In this paper, a precise and holistic flux and color control scheme based on nonlinear empirical models for practical closed-loop RGB LED systems are presented. These models account for the highly nonlinear relationship of the thermal interdependencies among the different types of LEDs mounted on the same heatsink. The mathematical relationships between the flux and color coordinates as a function of the reference voltages in a closed-loop system are analytically derived. The proposed tricolor control method is implemented using a real SITO LED driver with feedback control. The experimental results corroborate that the model predictions of flux and color points are in good agreement with the measurement results.

References

[1] O. Noboru, *Colorimetry: Fundamentals and Applications*. NewYork, NY, USA: Wiley, 2006.

[2] Y. Gu, N. Narendran, T. Dong, and H.Wu, "Spectral and luminous efficacy change of high-power LEDs under different dimming methods," *Proc. SPIE*, vol. 6337, p. 63370J, 2006.

[3] J. Garcia, M. Dalla-Costa, J. Cardesin, J. Alonso, and M. Rico-Secades, "Dimming of high-brightness LEDs by means of luminous flux thermal estimation," *IEEE Trans. Power Electron.*, vol. 24, no. 4, pp. 1107–1114, Apr. 2009.

[4] J. Lalith, Y. M. Gu, and N. Nadarajah, "Characterization of thermal resistance coefficient of high-power LEDs," in *Proc. 6th Int. Conf. Solid State Lighting*, San Diego, CA, Aug. 2006, pp. 63370–63377.

[5] J. Garcia, D. G. Lamar, M. A. Costa, J. M. Alonso, and M. R. Secades, "An estimator of luminous flux for enhanced control of high brightness LEDs", in *Proc. IEEE PESC 2008*, Rhodes, Greece, pp. 1852–1856, Jun. 2008.

[6] C. Biber, "LED light emission as a function of thermal conditions," in *Proc. IEEE Semicond. Thermal Meas. Manag. Symp.*, San Jose, CA, pp. 180–184, Mar. 2008.

[7] S. Y. R. Hui, and Y. X. Qin, "A general photo-electro-thermal theory for light emitting diode (LED) systems", *IEEE Trans. Power Electron.*, vol. 24, no. 8, pp. 1967–1976, Aug. 2009.

[8] X. Tao, and S. Y. R. Hui, "A general photo-electro-thermal-temporal theory for light-emitting diode (LED) systems", in *Proc. IEEE ECCE* 2010, pp. 184–191, Sep. 2010.

[9] K. H. Loo, Y. M. Lai, S. C. Tan, and C. K. Tse, "On the color stability of phosphor-converted white LEDs under DC, PWM, and bilevel drive," *IEEE Trans. Power Electron.*, vol. 27, no. 2, pp. 974–984, Feb. 2012.

[10] X. Tao, S. Y. R. Hui, "Dynamic photoelectrothermal theory for light

emitting diode systems", *IEEE Trans. Industrial Electron.*, vol. 59, no. 4, pp. 1751–1759, Apr. 2012.

[11] H.-T. Chen, D.-Y. Lin, S.-C. Tan, and S. Y. R. Hui, "Chromatic, photometric and thermal modeling of LED systems with nonidentical LED devices", vol. 29, no. 12, pp. 6636–6647, Dec. 2014.

[12] H.-T. Chen, S. Tan, and S. Hui, "Nonlinear dimming and correlated color temperature control of bi-color white LED systems," *IEEE Trans. Power Electron.*, vol. 30, no. 12, pp. 6934–6947, Dec. 2015.

[13] H.-T. Chen, S.-C. Tan, A. T. L. Lee, D.-Y. Lin, and S. Y. R. Hui, "Precise color control of red-green-blue light-emitting diode systems", *IEEE Trans. Power Electron.*, vol. 32, no. 4, pp. 3063–3074, Apr. 2017.

[14] A. T. L. Lee, H. Chen, S.-C. Tan, and S. Y. R. Hui, "Precise dimming and color control of LED systems based on color mixing", *IEEE Tran. Power Electron.*, vol. 31, no. 1, pp. 65–80, Jan. 2016.

[15] A. T. L. Lee, H. Chen, S.C. Tan, and S. Y. R. Hui, "Non-linear feedback control of robust bi-color LED lighting", *2015 IEEE Energy Conversion Congr. and Expo. (ECCE)*, pp. 3215-3222, Sep. 2015.

[16] D. Ma, W.-H. Ki, and C.-Y. Tsui, "A pseudo-CCM/DCM SIMO Switching converter with freewheel switching, " *IEEE J. Solid-State Circuits*, vol. 38, no. 6, pp. 1007–1014, Jun. 2003.

[17] D. Ma, W.-H. Ki, C.-Y. Tsui, and P. K. T. Mok, "Single-inductor multiple-output switching converters with time- multiplexing control in discontinuous conduction mode," *IEEE J. Solid-State Circuits*, vol. 38, no. 1, pp. 89–100, Jan. 2003.

[18] D. Kwon and G. A. Rincon-Mora, "Single-inductor-multiple-output switching DC-DC converters," *IEEE Trans. Circuits Syst. II, Express Briefs*, vol. 56, no. 8, pp. 614–618, Aug. 2009.

[19] A. Lee, J. Sin, and P. Chan, "Scalability of quasi-hysteretic FSM-based digitally-controlled single-inductor dual-string buck LED driver to multiple string," *IEEE Trans. Power Electron.*, vol. 29, no. 1, pp. 501–513, Jan. 2014.

[20] Y. Zhang and D. Ma, "A fast-response hybrid SIMO power converter with adaptive current compensation and minimized cross-regulation," *IEEE J. Solid-State Circuits*, vol. 49, no. 5, pp. 1242–1255, May 2014.

[21] W. Sun, C. Han, M. Yang, S. Xu, and S. Lu, "A ripple control dual-mode single-inductor dual-output buck converter with fast transient response," *IEEE Trans. Very Large Scale Integr. Syst.*, vol. 23, no. 1, pp. 107–117, Jan. 2015.

[22] C.-W. Chen and A. Fayed, "A low-power dual-frequency SIMO buck converter topology with fully-integrated outputs and fast dynamic operation in 45 nm CMOS," *IEEE J. Solid-State Circuits*, vol. 50, no. 9, pp. 2161–2173, Sep. 2015.

[23] K. Modepalli and L. Parsa, "A scalable N-color LED driver using single inductor multiple current output topology", *IEEE Trans. Power Electron.*, vol. 31, no. 5, pp. 3773–3783, May 2016.

[24] Y. Zheng, M. Ho, J. Guo, K.-L. Mak, and K. Leung, "A single-inductor multiple-output auto-buck-boost DC-DC converter with autophase allocation," *IEEE Trans. Power Electron.*, vol. 31, no. 3, pp. 2296–2313, Mar. 2016.

[25] Y. Guo, S. Li, A. Lee, S.-C. Tan, C. K. Lee, and S. Y. R. Hui, "Single stage AC/DC single-inductor multiple-output LED drivers, " *IEEE Trans. Power Electron.*, vol. 31, no. 8, pp. 5837–5850, Aug. 2016.

[26] G. Yue, A. T. L. Lee, S. Li, S. C. Tan, C. K. Lee, and S. Y. R. Hui, "AC-DC single-inductor multiple-output (SIMO) LED drivers, U.S. Patent US10212770B2, 2019.

[27] Datasheet: TMS320F28335, "TMS320F2833x, TMS320F2823x digital signal controllers (DSCs)", SPRS439O, Texas Instrument, Apr. 2019.

[28] User's Manual: PMS-50/80, "PMS-50/80 UV-VIS-near IR Spectrophoto-colorimeter", version 3.0, Everfine Photo-E-Info Co., Ltd., 2009.

[29] E. F. Schubert, *Light-Emitting Diodes*, 2nd edition, Cambridge: Cambridge University Press, 2006.

[30] American National Standard, Specifications for Chromaticity of Solid State Lighting Products, ANSI C78.377 (American National Standards Institute, 2008).

[31] P. Deurenberg, C. Hoelen, J. V. Meurs, and J. Ansems, "Achieving color point stability inRGBmulti-chip LED modules using various color control loops," in *Proc. SPIE, 5th Int. Conf. Solid State Lighting*, Sep. 2005, vol. 5941, pp. 63–74.

[32] T. P. Sun and C. H. Wang, "Specially designed driver circuits to stabilize LED light output without a photodetector," *IEEE Trans. Power Electron.*, vol. 27, no. 9, pp. 4140–4152, Sep. 2012.

APPENDIX

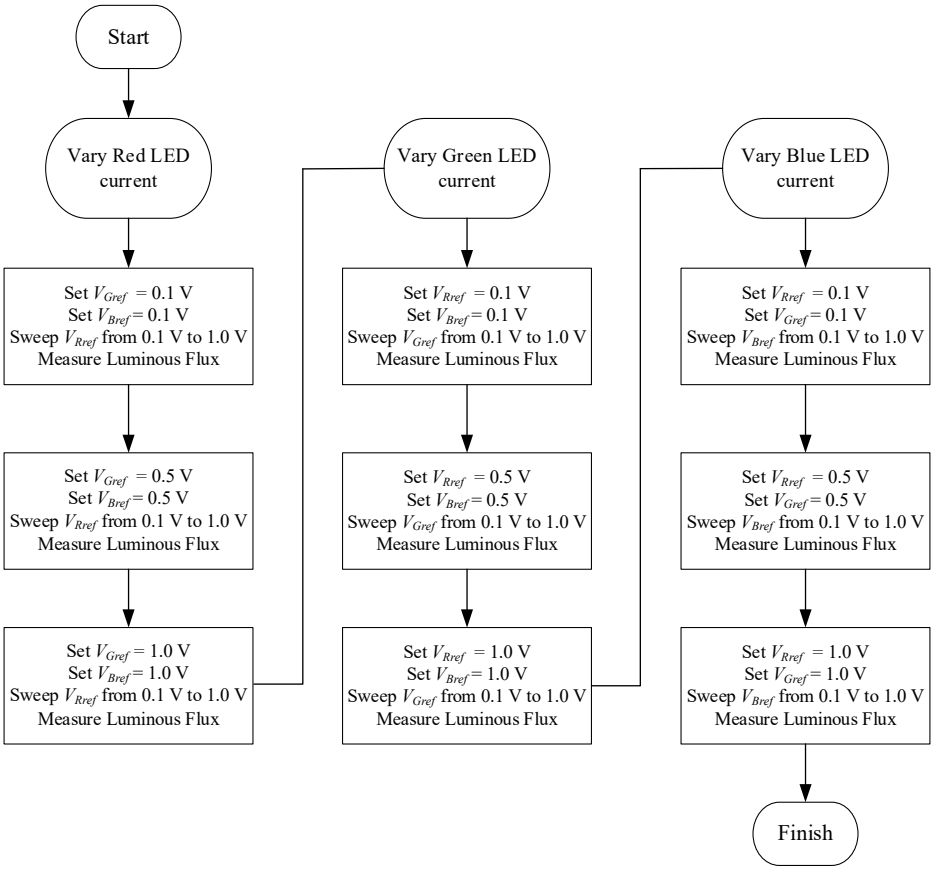

Fig. A1. Flowchart to illustrate the procedures of obtaining the proposed empirical luminous flux model.

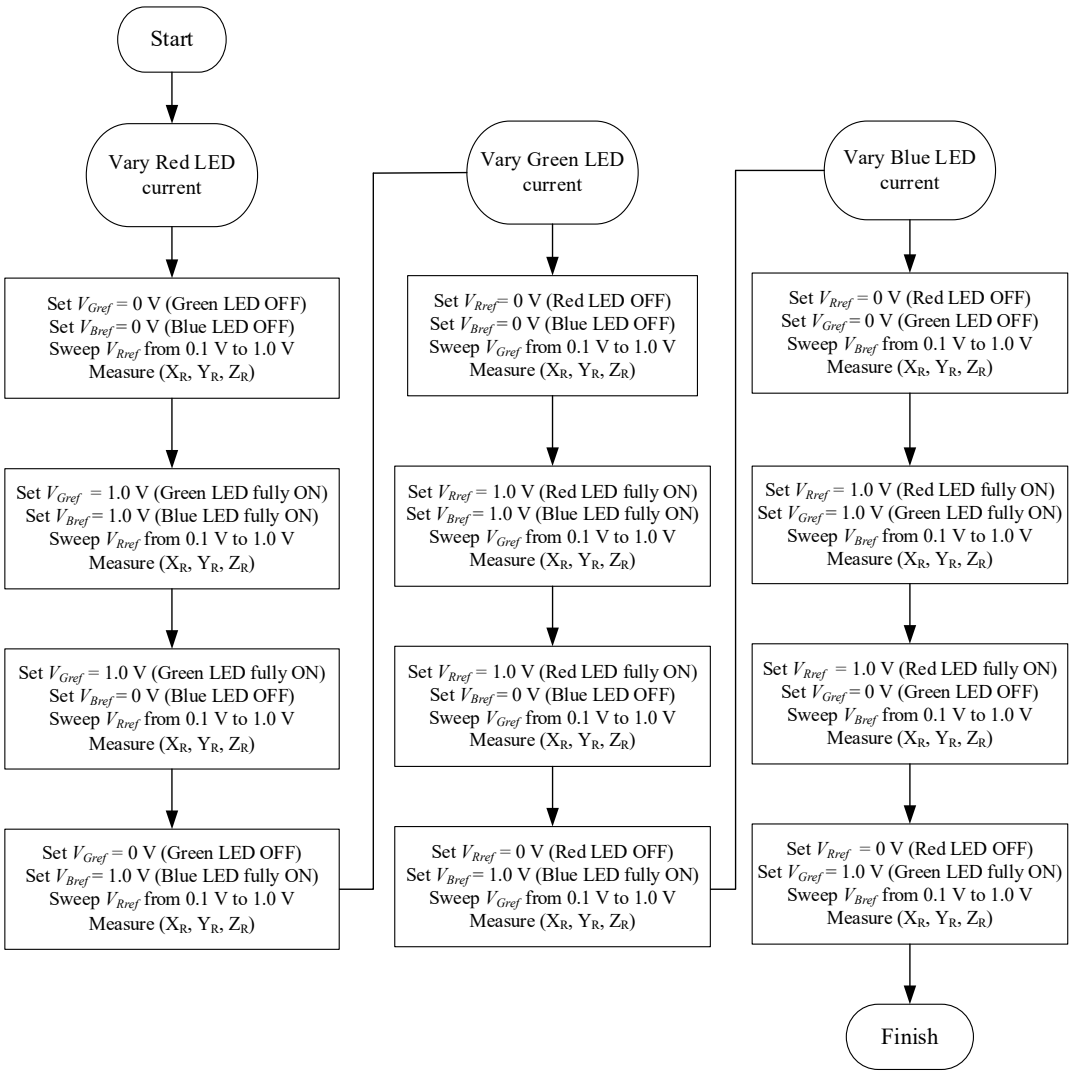

Fig. A2. Flowchart to illustrate the procedures of obtaining the proposed empirical color model.